



Republic of Iraq  
Ministry of Higher Education and Scientific Research  
University of Technology  
Department of Building and Constructions Engineering



# **Assessment of Ground Water Pressure Effects Around The Tunnel of Baghdad Metro**

A Thesis  
Submitted to The Department of Building and Constructions  
Engineering of The University of Technology  
in Partial Fulfillment of The Requirements  
for The Degree of Doctor of Philosophy  
in Water Resources Engineering

By

**Muammar Hazim Ali Al-Taee**  
(M. Sc. Water Resources Engineering)

Supervised By

**Prof. Dr. Aqeel Shaker Al-Adili**  
**Assoc. Prof. Dr. Nagaratnam Sivakugan/James Cook**  
**University/Australia**

January 2018 A. D.

Rabeea Al-Thanee 1439 A. H.

بِسْمِ اللّٰهِ الرَّحْمٰنِ الرَّحِیْمِ

{ وَضَرَبَ لَنَا مَثَلًا وَنَسِيَ خُلُقَهُ قَالَ مَنْ يُحْيِي الْعِظَامَ وَهِيَ رَمِيمٌ ﴿٧٨﴾ قُلْ يُحْيِيهَا الَّذِي أَنْشَأَهَا أَوَّلَ مَرَّةٍ وَهُوَ بِكُلِّ

خَلْقٍ عَلِيمٌ {

صَدَقَ اللّٰهُ الْعَلِيِّ الْعَظِيمِ

يس (٧٨-٧٩)

## Dedication

- To my teacher who spent his life to be a beacon of my way .....
- To the memory of my dear brother Muhammad who left the life at his youth ..
- To my family, especially my dear son MuhammadBaqer .....
- To my dear parents, my brothers, and my sisters .....
- To the memory of Dr. Salah Tawfeek Ali Al-Bazaz who was my supervisor in M. Sc. and I learnt from him the valuable information in science .....
- To all people who love me and all that I love deeply .....



**Muammar Hazim Ali Al-Taee**

**January 2018**

## **Acknowledgements**

Praise be to **ALLAH** who enabled me to complete this work under his benediction.

I would like to express my thanks to my supervisors Prof. Dr. Aqeel Shaker Al-Adili and Assoc. Prof. Dr. Nagaratnam Sivakugan from the College of Science, Technology, and Engineering in the James Cook University, Australia.

Cordial thanks and deepest gratitude to Asst. Prof. Dr. Saad Faek in the Building and Constructions Engineering Department in the University of Technology for his valuable guidance in the geotechnical aspects throughout the preparation of this work.

I am indebted to the General Commission for Ground Water (GCGW), especially to Dr. Ahmed Nadhom, and the National Center for Water Resources Management in Iraq (NCWRM), especially to Engineer Hamdiea Al-Khafaji, for giving me the data of ground water that have been used in this study and further information were useful for me.

I am also grateful to the National Center for Construction Labs and Researches (NCCLR) for unforgettable help in collecting the information of the proposed Baghdad metro from the Soil Investigation Reports conducted for this proposed project.

I would also like to express my thanks to the Mayoralty of Baghdad, especially to Engineer Firas Shafeek Abbas in the Roads Department who allowed me to see the documents of the newest study conducted by French firm Systra for the proposed Baghdad metro in 2013.

I also record my thanks to my dear friend Dr. Riyadh Jasim Al-Saadi for his kindly support throughout this work and anyone helped me in this work.

Finally, sincere gratitude and appreciation to my family for their encouragement and support during the study.



**Muammar Hazim Ali Al-Taee**

**January 2018**

## **Abstract**

In this study a three dimensional numerical analysis by using the finite element method has been performed to predict the field variables of the soil around the proposed tunnel (Baghdad metro) which consists of two lines in Baghdad city with two routes for each line. The first line lies in Rasafa and the second line extends from Rasafa to Karkh. Abaqus 2016, was used to simulate the behaviour of the two routes of the proposed Baghdad metro by using a fully coupled three dimensional stress-pore pressure model at 38 locations, where 18 and 20 locations on the first and the second lines, were selected respectively. The ground water table depths at these locations were determined by using best of the best spatial raster surfaces generated from ground surface elevations and static water levels recorded at 206 wells in Baghdad Governorate using ArcGIS10.5 package. The soil layers were assumed to be an elasto-plastic materials conforming to the Mohr-Coulomb failure criterion together with the nonassociated flow rule and the shotcrete liners were assumed to behave in a linear elastic manner.

The actual tunnelling processes of the proposed Baghdad metro in each model were closely simulated before, during, and after tunnel excavation by using Model Change Method (MCM) where the tunnel was assumed to be fully excavated.

The vertical displacements of the soil surrounding liners of the two tunnel routes in the deformed shapes of three dimensional stress-pore pressure coupled models for those 38 locations have been computed during and after tunnel excavation. It was found that maximum downward vertical displacements occurred at the crown points of the two tunnel routes at location-8/line-1 near Army canal of about 114.4 mm at the end of the excavation step and so on for long term after completing the linings installation step. Then, maximum upward vertical displacements occurred at the invert points of the two tunnel routes in the

same location about 116.6 mm at the end of the excavation step and so on for long term after completing the linings installation step.

For the proposed Baghdad metro under Tigris River, model of location-11 (under Tigris)/line-2 was used to compute pore water pressures at the soil surrounding liners of the two tunnel routes and at the bed of river during and after tunnel excavation. Firstly, the pore water pressures at the soil surrounding the two liners in the deformed shape of this model were computed. It was found that all pore water pressures at the end of the excavation step were negative with range approximately from 0.4 kN/m<sup>2</sup> to 1.7 kN/m<sup>2</sup> and at the end of the linings installation step were positive with range approximately from 74.1 kN/m<sup>2</sup> to 140 kN/m<sup>2</sup>. Then, they were about 317.7 kN/m<sup>2</sup> along the crown paths and 383.45 kN/m<sup>2</sup> along the invert paths of the two tunnel routes after one year from the end of the lining installation step and so on for long term. Secondly, the pore water pressures at the river bed were computed in the deformed shape of the same model of location-11 (under Tigris)/line-2 during and after tunnel excavation. It was found that all pore water pressures at this bed along the middle distance between the two tunnel routes at the end of the excavation and linings installation steps were about 2 kN/m<sup>2</sup> smaller than those pressures generated from the water depth in the river at the geostatic step which was considered equal to 6 m. Then, it was found that the water depth in the river rebounded to its level at the geostatic step approximately after one year from the end of the lining installation step and so on for long term.

In this study, it has been found that the fully coupled three dimensional stress-pore pressure model realistically captures the mechanical and hydrological interaction between the proposed Baghdad metro and ground water. It was found that no risks have been happened on the ground surface and depth of water in Tigris at all selected locations.

## Supervisors Certificate

We certify that the preparation of this thesis entitled “**Assessment of Ground Water Pressure Effects Around The Tunnel of Baghdad Metro**”, was prepared by **Muammar Hazim Ali Al-Tae** under our supervision at the Department of Building and Construction Engineering of the University of Technology, in partial fulfillment of the requirements for the **Degree of Doctor of Philosophy** in Water Resources Engineering.

Signature:   
**Prof. Dr. Aqeel Al-Adili**

Date: 9 / 1 / 2018

Signature:

**Assoc. Prof. Dr. Nagaratnam Sivakugan**

Date: / / 2018

In the view of the available recommendation, I forward this thesis for the debate by the Examining Committee.


Signature:   
**Asst. Prof. Dr. Mahmoud Saleh Al-Khafaji**

The head of Water and Hydraulic Structures Engineering Branch


Date: 9 / 1 / 2018


## Examining Committee Certificate


We certify that we have read this thesis entitled "Assessment of Ground Water Pressure Effects Around The Tunnel of Baghdad Metro", and as an examining committee, we examined the student **Muammar Hazim Ali Al-Tae** in its contents and in what is connected with it, and that in our opinion it meets the standard of a thesis for the **Degree of Doctor of Philosophy** in Water Resources Engineering.

Signature:   
Prof. Dr. Aqeel Al-Adili  
Date: 9 / 1 / 2018  
(Supervisor)

Signature:  
Assoc. Prof. Dr. Nagaratnam Sivakugan  
Date: / / 2018  
(Supervisor)

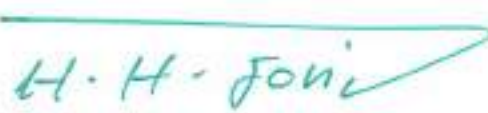
Signature:   
Asst. Prof. Dr. Nahla M. Salim  
Date: 9 / 1 / 2018  
(Member)

Signature:   
Asst. Prof. Dr. Thair Sharif Khayyun  
Date: 9 / 1 / 2018  
(Member)

Signature:   
Asst. Prof. Dr. Jaafar S. Maatooq  
Date: 8 / 1 / 2018  
(Member)

Signature:   
Asst. Prof. Dr. Alaa Hussain Al-Shami  
Date: 9 / 1 / 2018  
(Member)

Signature:   
Name: Prof. Dr. Riyadh Zuhair Azzubaidi  
Date: 11 / 1 / 2018  
(Chairman)

Signature:   
Asst. Prof. Dr. Hasan Hamodi Joni  
Date: 20 / 1 / 2018  
The head of Building and Constructions Engineering Department.



## List of Contents

<b><u>Subject</u></b>	<b><u>Page</u></b>
Didication .....	iii
Acknowledgements .....	iv
Abstract .....	v
Supervisors Certificate .....	vii
Examining Committee Certificate .....	viii
List of Contents .....	ix
List of Tables .....	xii
List of Figures .....	xiv
List of Symbols .....	xxi
List of Abbreviations and Acronyms .....	xxiii
Chapter One: Introduction .....	1
1.1 Prelude .....	1
1.2 Objectives of The Present Study .....	3
Chapter Two: Review of Literature .....	4
2.1 Previous Studies on Simulation of Tunnelling Using Abaqus .....	4
2.2 Previous Studies on Simulation of The proposed Baghdad Metro ..	10
2.3 Spatial Interpolation Techniques .....	14
2.4 Stress-Pore Pressure Coupled Analysis .....	15
Chapter Three: Description of The Proposed Baghdad Metro .....	19
3.1 Layout and Geometry of The Proposed Baghdad Metro .....	19
3.2 Ground Water Level in Baghdad .....	28
3.3 Description of The Selected Locations in Modelling .....	31
3.3.1 Ground Water Table Depths .....	36
3.3.2 Soil Strata .....	41
Chapter Four: Coupled Stress-Pore Pressure Modelling of The Proposed Baghdad Metro .....	45
4.1 General Description for Getting Started with Abaqus .....	45

## **List of Contents, Cont.**

4.1.1 Definition of Abaqus .....	45
4.1.2 Stages of Abaqus Analysis .....	47
4.1.3 Components of An Abaqus Analysis Model .....	48
4.2 Coupled Stress-Pore Pressure Models of The Proposed Baghdad Metro .....	51
4.2.1 Extensions of The Finite Element Mesh .....	51
4.2.2 Discretization of The Model .....	54
4.2.3 Definition of Initial and Boundary Conditions .....	56
4.2.4 Constitutive Modelling (Material Modelling) .....	58
4.2.5 Simulation Procedure of The Proposed Baghdad Metro .....	58
4.2.6 Analysis of Field Variables of The Proposed Baghdad Metro	61
Chapter Five: Results and Analysis .....	66
5.1 Vertical Displacements of Soil Surrounding Liners .....	66
5.2 Pore Water Pressures at Location Under Tigris .....	71
5.2.1 Distribution of Pore Water Pressures .....	71
5.2.2 Pore Water Pressures of Soil Surrounding Liners .....	77
5.2.3 Comprehensive Analysis for PWP's of Soil Surrounding Liners .....	92
5.3 Water Depth Response in Tigris Due to Tunnelling .....	95
5.4 Comprehensive Analysis for Water Depth Response in Tigris Due to Tunnelling .....	108
Chapter Six: Conclusions and Recommendations .....	112
6.1 Conclusions .....	112
6.2 Recommendations .....	115
References .....	117
Appendix A: Information of 206 Wells for Baghdad Governorate.	
Appendix B: Soil Strata Properties for 37 Locations on The Proposed Baghdad Metro.	

### **List of Contents, Cont.**

Appendix C: Initial Conditions of Pore Water Pressures and Effective Stresses of Three Dimensional models for 37 Locations on The Proposed Baghdad Metro.

Appendix D: Change Curves of The Vertical Displacements ( $U_3$ ) of The Front Crown and Invert Points During and After Tunnel Excavation for 37 Locations on The Proposed Baghdad Metro.

## List of Tables

<u>Table</u>	<u>Title</u>	<u>Page</u>
Table 3.1	Field information for the locations of the proposed Baghdad metro/line-1 selected in modelling, with referencing to Figure 3.5 .....	35
Table 3.2	Field information for the locations of the proposed Baghdad metro/line-2 selected in modelling, with referencing to Figure 3.5 .....	35
Table 3.3	RMSE between observed and predicted GSEs and SWLs in Baghdad Governorate and Baghdad City .....	37
Table 3.4	Ground water depths at the locations of the proposed Baghdad metro/line-1 selected in modelling .....	40
Table 3.5	Ground water depths at the locations of the proposed Baghdad metro/line-2 selected in modelling .....	40
Table 3.6	Coordinates of the locations selected in modelling for the proposed Baghdad metro/line-1 and the boreholes as accurately as near to them .....	42
Table 3.7	Coordinates of the locations selected in modelling for the proposed Baghdad metro/line-2 and the boreholes as accurately as near to them .....	42
Table 3.8	Soil strata properties for location-1/line-1 of the proposed Baghdad metro, with returning to $Z_{invert}$ mentioned in Table 3.1 .....	44
Table 4.1	Dimensions of the finite element meshes for the locations of the proposed Baghdad metro selected for simulation .....	53
Table 4.2	Numbers of elements and nodes of the finite element meshes for the locations selected for simulation for the proposed Baghdad metro/line-1 .....	54

## List of Tables, Cont.

<u>Table</u>	<u>Title</u>	<u>Page</u>
Table 4.3	Numbers of elements and nodes for three dimensional finite models of locations on Baghdad metro line-2 selected for simulation .....	55
Table 4.4	Initial conditions of pore water pressures and effective stresses of the three dimensional finite element model for location-1/line-1, with referencing to Table 3.8 .....	57
Table A.1	Available information of 206 wells for Baghdad Governorate within the last decade .....	A-1
Tables B.1-B.37	Soil Strata Properties for 37 Locations on The Proposed Baghdad Metro .....	B-1 to B-22
Tables C.1-C.37	Initial Conditions of Pore Water Pressures and Effective Stresses of Three Dimensional models for 37 Locations on The Proposed Baghdad Metro .....	C-1 to C-13

## List of Figures

<b><u>Figure</u></b>	<b><u>Title</u></b>	<b><u>Page</u></b>
Figure 3.1	Iraqi map showing Baghdad and adjacent governorates .....	19
Figure 3.2	Map of Baghdad Governorate with its administrative regions	21
Figure 3.3	Map of Baghdad Governorates with satellite image of Baghdad City (60 cm error) .....	22
Figure 3.4	Layout of Baghdad metro plotting on satellite image of Baghdad City (60 cm error) .....	23
Figure 3.5	Typical vertical depth for two routes of Baghdad metro (source of proposed dimensions is Mayoralty of Baghdad, 2013) .....	26
Figure 3.6	Layout of Baghdad metro with supplementary routes plotting on satellite image of Baghdad City (60 cm error) .....	27
Figure 3.7	Distribution of 206 wells for Baghdad Governorate .....	29
Figure 3.8	Distribution of 49 wells within Baghdad City on satellite image (60 cm error) .....	30
Figure 3.9	The locations of the proposed Baghdad metro selected in modelling plotting on satellite image for Baghdad City (60 cm error) .....	32
Figure 3.10	The locations of the proposed Baghdad metro/line-1 selected in modelling .....	33
Figure 3.11	The locations of the proposed Baghdad metro/line-2 selected in modelling .....	34
Figure 3.12	Spatial raster surface for GSEs in Baghdad City obtained from the IDW interpolation method .....	38
Figure 3.13	Spatial raster surface for SWLs in Baghdad City obtained from the IDW interpolation method .....	39
Figure 4.1	Stages of Abaqus analysis .....	48

## List of Figures, Cont.

<u>Figure</u>	<u>Title</u>	<u>Page</u>
Figure 4.2	(A) Finite element model of typical location for the proposed Baghdad metro with referencing to Figure 3.5; (B) Diameters of tunnel; (C) Horizontal distance between the two tunnel routes .....	53
Figure 4.3	(A) Layout of the observation points at the upper surface and the front face of deformed three dimensional finite element model for a typical location of the proposed Baghdad metro; (B) Layout of the observation points around tunnel section ....	64
Figure 4.4	(A) Layout of the observation paths at the upper surface of deformed three dimensional finite element model for a typical simulation step at location -11(under Tigris)/line-2 of the proposed Baghdad metro; (B) Layout of the observation paths around tunnel section .....	65
Figure 5.1	Change curves of the vertical displacements (U3) for the front faces of the left and right routes at location-1/line-1 during excavation (10 days), linings installation (30 hours), and consolidation (10 days) steps .....	67
Figure 5.2	Spatial variation of the vertical displacements at the crown and invert points of the left and right routes of the proposed Baghdad metro/line-1 at the end of the excavation, linings installation, and consolidation steps .....	69
Figure 5.3	Spatial variation of the vertical displacements at the crown and invert points of the left and right routes of the proposed Baghdad metro/line-2 at the end of the excavation, linings installation, and consolidation steps .....	70

## List of Figures, Cont.

<u>Figure</u>	<u>Title</u>	<u>Page</u>
Figure 5.4	Distribution of vertical displacements of the soil media within the deformed three dimensional model of location-11 (under Tigris)/line-2 at the geostatic step .....	73
Figure 5.5	Distribution of pore water pressures (KN/m <sup>2</sup> ) of the soil media within the deformed three dimensional model of location-11 (under Tigris)/line-2 at the geostatic step .....	73
Figure 5.6	Distribution of pore water pressures (KN/m <sup>2</sup> ) of the soil media within the deformed three dimensional model of location-11 (under Tigris)/line-2 at the end of the excavation step .....	74
Figure 5.7	Distribution of pore water pressures (KN/m <sup>2</sup> ) of the soil media within the deformed three dimensional model of location-11 (under Tigris)/line-2 at the end of the linings installation step .....	75
Figure 5.8	Distribution of pore water pressures (KN/m <sup>2</sup> ) of the soil media within the deformed three dimensional model of location-11 (under Tigris)/line-2 at end of the consolidation step .....	76
Figure 5.9	Change curves of PWP for the front face of the left route at location-11 (under Tigris)/line-2 during the excavation step (10 days) .....	78
Figure 5.10	Change curves of PWP for the rear face of the left route at location-11 (under Tigris)/line-2 during the excavation step (10 days) .....	78
Figure 5.11	Change curve of PWP along the crown and invert paths of the left route at location-11 (under Tigris)/line-2 at the end of the excavation step .....	78



## List of Figures, Cont.

<u>Figure</u>	<u>Title</u>	<u>Page</u>
Figure 5.12	Change curves of PWP's for the front face of the right route at location-11 (under Tigris)/line-2 during the excavation step (10 days) .....	79
Figure 5.13	Change curves of PWP's for the rear face of the right route at location-11 (under Tigris)/line-2 during the excavation step (10 days) .....	80
Figure 5.14	Change curve of PWP along the crown and invert paths of the right route at location-11 (under Tigris)/line-2 at the end of the excavation step .....	80
Figure 5.15	Graphical comparison between the change curves of PWP's for the front and rear faces of the left and right routes at location-11 (under Tigris)/line-2 during the excavation step (10 days) .....	82
Figure 5.16	Graphical comparison between the change curves of PWP's for the crown and invert paths of the left and right routes at location-11 (under Tigris)/line-2 at the end of the excavation step .....	82
Figure 5.17	Change curves of PWP's for the front and rear faces of the left route at location-11 (under Tigris)/line-2 during the linings installation step (30 hours) .....	83
Figure 5.18	Change curve of PWP along the crown and invert paths of the left route at location-11 (under Tigris)/line-2 at the end of the lining installation step .....	83
Figure 5.19	Change curves of PWP's for the front and rear faces of the right route at location-11 (under Tigris)/line-2 during the linings installation step (30 hours) .....	84

## List of Figures, Cont.

<u>Figure</u>	<u>Title</u>	<u>Page</u>
Figure 5.20	Change curve of PWP along the crown and invert paths of the right route at location-11 (under Tigris)/line-2 at the end of the lining installation step .....	85
Figure 5.21	Graphical comparison between the change curves of PWPs for the front and rear faces of the left and right routes at location-11 (under Tigris)/line-2 during the linings installation step (30 hours) .....	86
Figure 5.22	Graphical comparison between the change curves of PWPs along the crown and invert paths of the left and right routes at location-11 (under Tigris)/line-2 at the end of the linings installation step .....	87
Figure 5.23	Change curves of PWPs for the front and rear faces of the left route at location-11 (under Tigris)/line-2 during the consolidation step (1 year) .....	88
Figure 5.24	Change curves of PWPs along the crown and invert paths of the left route at location-11 (under Tigris)/line-2 at the end of the consolidation step .....	88
Figure 5.25	Change curves of PWPs for the front and rear faces of the right route at location-11 (under Tigris)/line-2 during the consolidation step (1 year) .....	89
Figure 5.26	Change curves of PWPs along the crown and invert paths of the right route at location-11 (under Tigris)/line-2 at the end of the consolidation step .....	89
Figure 5.27	Graphical comparison between the change curves of PWPs for the front and rear faces of the left and right routes at location-11 (under Tigris)/line-2 during the consolidation step (1 year) .....	91

## List of Figures, Cont.

<u>Figure</u>	<u>Title</u>	<u>Page</u>
Figure 5.28	Graphical comparison between the change curves of PWP's for the crown and invert paths of the left and right routes at location-11 (under Tigris)/line-2 at the end of the consolidation step .....	91
Figure 5.29	Combination of Figure 5.15, 5.21, and 5.27 (the acronyms in this figure are mentioned in Figure 4.3 and in the List of Abbreviations and Acronyms) .....	94
Figure 5.30	Change curve of PWP's for Tigris bed at location-11 (under Tigris)/line-2 during the excavation step (10 days) .....	97
Figure 5.31	Change curves of PWP's for Tigris bed at location-11 (under Tigris)/line-2 at the end of the excavation step .....	98
Figure 5.32	Graphical comparison between the change curves of PWP's for Tigris bed at location-11 (under Tigris)/line-2 during the excavation step (10 days) .....	99
Figure 5.33	Graphical comparison between the change curves of PWP's for Tigris bed at location-11 (under Tigris)/line-2 at the end of the excavation step .....	100
Figure 5.34	Change curves of PWP's for Tigris bed at location-11 (under Tigris)/line-2 during the linings installation step (30 hours) ...	101
Figure 5.35	Change curves of PWP's for Tigris bed at location-11 (under Tigris)/line-2 at the end of the linings installation step .....	102
Figure 5.36	Graphical comparison between the change curves of PWP's for Tigris bed at location-11 (under Tigris)/line-2 during the linings installation step (30 hours) .....	103
Figure 5.37	Graphical comparison between the change curves of PWP's for Tigris bed at location-11 (under Tigris)/line-2 at the end of the linings installation step .....	104

## List of Figures, Cont.

<u>Figure</u>	<u>Title</u>	<u>Page</u>
Figure 5.38	Change curves of PWP's for Tigris bed at location-11 (under Tigris)/line-2 during the consolidation step (1 year) .....	105
Figure 5.39	Change curves of PWP's for Tigris bed at location-11 (under Tigris)/line-2 at the end of the consolidation step .....	106
Figure 5.40	Graphical comparison between the change curves of PWP's for Tigris bed at location-11 (under Tigris)/line-2 during the consolidation step (1 year) .....	107
Figure 5.41	Graphical comparison between the change curves of PWP's for Tigris bed at location-11 (under Tigris)/line-2 at the end of the consolidation step .....	108
Figure 5.42	Combination of Figure 5.32, 5.36, and 5.40 (the acronyms in this figure are mentioned in Figure 4.3 and in the List of Abbreviations and Acronyms) .....	110
Figures D.1-D.37	Change Curves of The Vertical Displacements (U <sub>3</sub> ) of The Front Crown and Invert Points During and After Tunnel Excavation for 37 Locations on The Proposed Baghdad Metro .....	D-1 to D-22

## List of Symbols

bar	Unit of pressure which is equal to 100 kPa.
$C$	Cohesion of soil ( $F/L^2$ ).
$D_i$	Inner diameter of tunnel (L).
$D_o$	Outer diameter of tunnel (L).
$e$	Void ratio (dimensionless).
$E$	Young's modulus of elasticity ( $F/L^2$ ).
$f$	All body forces except the weight of the wetting liquid (F)
$\hat{f}$	Body forces per unit volume ( $F/L^3$ ).
$f_w$	Weight of the wetting liquid (F).
$g$	Gravitational acceleration ( $L^2/T$ ).
$\hat{k}$	Permeability of the medium (L/T).
$K$	Coefficient of permeability (L/T).
$K_0$	Coefficient of lateral earth pressure at rest (dimensionless).
$K_a$	Active lateral earth pressure coefficient (dimensionless).
$n$	Porosity.
$n_t$	Volume of trapped wetting liquid per unit of current volume.
$S$	Surface under consideration ( $L^2$ ).
$s$	Degree of saturation.
$t$	Time (T), surface tractions per unit area.
$U_3$	Vertical displacement (L).
$v_w$	Velocity of the wetting liquid (L).
$x$	Unit vector in x-direction.
$X$	Projected coordinate in X-direction (L).
$Y$	Projected coordinate in Y-direction (L).
$X_{\text{mesh}}$	Extension of mesh in X-direction (L).
$Y_{\text{mesh}}$	Extension of mesh in Y-direction (L).
$Z_{\text{invert}}$	Vertical distance from the ground surface to the invert point in the outer diameter of tunnel (L).

## List of Symbols, Cont.

$Z_{\text{mesh}}$	Extension of mesh in Z-direction (L).
$\rho_w^o$	Density of the liquid in the reference configuration ( $\text{FT}^2/\text{L}^4$ ).
$\delta u_w$	arbitrary, continuous, variation field.
$\delta v$	Virtual velocity field (L).
$\delta \varepsilon$	Virtual rate of deformation (L).
$\nu$	Poisson's ratio (dimensionless).
$\rho$	Mass density ( $\text{FT}^2/\text{L}^4$ ).
$\rho_d$	Dray mass density ( $\text{FT}^2/\text{L}^4$ ).
$\rho_s$	Saturated mass density ( $\text{FT}^2/\text{L}^4$ ).
$\rho_w$	Unit weight of water ( $\text{FT}^2/\text{L}^4$ ).
$\sigma$	True (Cauchy) stress ( $\text{F}/\text{L}^2$ ).
$\Phi$	Piezometric head (L).
$\phi$	Angle of internal friction (degree).

## List of Abbreviations and Acronyms

.dat	Data file.
.fil	Results file.
.inp	Input file.
.odb	Output database file.
.res	Restart file.
3D	Three dimensional.
a.s.l.	Above sea level.
C3D8R	Stress-displacement eight nodes linear brick elements with reduced integration and with hourglass control.
C3D8RP	Eight nodes trilinear displacement and pore pressure elements with reduced integration.
CAE	Complete Abaqus Environment.
CFD	Computational Fluid Dynamics
cm	Centimeter.
Cont.	Continuous.
E	East.
FE	Finite element.
FRP	Fiber reinforced pipes
G.S.	Ground surface.
GCGW	General Commission of Ground Waters
GIS	Geographic Information Systems.
GSE	Ground surface elevation.
GSEs	Ground surface elevations.
HF4	High Frequency from fourth degree.
HM	Coupled hydro-mechanical behaviour
hr	Hour.
IDW	Inverse Distance Weighted.
Inc.	Incorporated.

## List of Abbreviations and Acronyms, Cont.

km	Kilometer.
kN	Kilonewton.
LR: Front c.p.	Left route: Front crown point.
LR: Front i.p.	Left route: Front invert point.
LR: Rear c.p.	Left route: Rear crown point.
LR: Rear i.p.	Left route: Rear invert point.
m	Meter.
N	North.
NATM	Austrian Tunnelling Method.
NCCLR	National Center for Constructions Laboratories and Researches.
NCWRMI	National Center for Water Resources Management in Iraq.
NN	Natural Neighbour.
no.	Number.
PWPs	Pore water pressures.
R. R.	Rail road.
RMSE	Root mean squared errors.
RR: Front c.p.	Right route: Front crown point.
RR: Front i.p.	Right route: Front invert point.
RR: Rear c.p.	Right route: Rear crown point.
RR: Rear i.p.	Right route: Rear invert point.
S	South.
s	Second.
SWL	Static water level.
SWLs	Static water levels.
TBM	Tunnel Boring Machine.
UF-left point	Upper front left point.
UF-middle point	Upper front middle point.
UF-right point	Upper front right point.



## **List of Abbreviations and Acronyms, Cont.**

UR-left point	Upper rear left point.
UR-middle point	Upper rear middle point.
UR-right point	Upper rear right point.
UTM	Universal Transverse Mercator.
W	West.
W.T.	Water table.
WGS	World Geodetic System.

# **Chapter One**

## **Introduction**

### **1.1 Prelude**

The constructions of tunnels are very complex because it involves precise and accurate planning. Tunnel construction depends mainly on geological study of the subsurface before determining the type of construction method and costing involves. This is because the type of soil formation will determine the structural needs, types of machineries, suitability for that particular location to construct the tunnel and also the environmental impact on the society and the natural surrounding especially the subsurface of the soils such as underground streams and the stability of the soil (Kannapiran, 2005).

“The effects of ground water in tunnelling are manifold. During tunnel excavation in a water-bearing ground, seepage flow towards the opening takes place because the pressure at the excavation boundary is, in general, atmospheric and the tunnel acts as a ground water drain. The seepage flow may lead to a drawdown of the water level, to a decrease in the discharge of wells, or to consolidation and substance. Besides these, in the broader sense, environmental impacts, larger water inflow may impede excavation works or have a serious impact on the serviceability of the tunnel during its operation phase” (quoted in Anagnostou, 2006). Tunnels can be drilled by a TBM to minimize inflows and ground water impacts, restricting the effect on the tunnel face. This method is especially suitable for urban tunnelling where the works are usually undertaken near the ground surface (Font-Capó, 2012).

The handling and control of ground water inflow presents one of the most frequent, hazardous, and troublesome problems encountered in tunnel and cut and cover construction. Although, these problems are usually more severe during actual construction, if not properly resolved they can be a source of continued

concern and expense throughout the life of the structure. While a certain amount of water inflow may be tolerated during construction, depending on the type of structure and construction methods employed such a condition may not be acceptable for long term usage of the structure. There are many factors that control the amount of ground water flow into a tunnel in the absence or failure of waterproofing methods. The height of the water table above the tunnel determines the water pressure, and the permeability of the ground affects the possible flow quantity. The extent in depth and size of the aquifer in which the tunnel is located and its distance from a possible source of recharge such as river, lake, etc. also affect possible flow (Scheffey, 1982).

Many previous studies were done on the proposed Baghdad metro on one typical location with assumed soil strata and their properties. Then, the soil strata were assumed to be fully saturated. All of these studies were used two dimensional numerical methods to analyze the behaviour of tunnel.

The present study aims to analyze behaviour of the tunnel of the proposed Baghdad metro at different locations before, during, and after tunnel excavation. The actual soil strata at these locations and their properties are adopted. The best predicted water table depths at these locations are depended. In order to realistically capture the interaction mechanism between the tunnel of the proposed Baghdad Metro and ground water at different locations, a three dimensional stress-pore pressure fully coupled formulation is adopted. The famous GIS software package ArcGIS 10.5 is used to generate best of the best spatial raster surfaces for ground surface elevations and static water levels to compute the water table depths at the locations selected on this metro.

There are a multitude of finite element packages can be used for simulation of tunnel such as Flac, Plaxis, Adina, Abaqus, etc. In this study, Abaqus is selected so as to take advantage of its effectiveness in stress-pore pressure coupled modelling as well as robustness in the numerical solution strategy for soil plasticity.

## **1.2 Objectives of The Present Study**

The main objectives of the present study are:

1. Computing the displacements of soil around the proposed Baghdad metro at crown and invert points of the tunnel at each location before, during, and after tunnel excavation.
2. Study and investigation of distributions of pore water pressures of the soil media within the model at the location under Tigris River before, during, and after tunnel construction. Then, pore water pressures values of the soil around the tunnel and at the Tigris will be also computed as time dependent values at observation points and as space dependent values along observation paths before, during, and after tunnel construction.
3. Study and observation of ground water table depths at different locations on the proposed Baghdad metro by using GIS software package, ArcGIS 10.5, to generate best spatial raster surfaces for ground surface elevations and best static water levels for Baghdad Governorate.
4. Analysis of effects of pore water pressures of the soil surrounding liners on the two tunnel routes under Tigris and water depth response in river. The displacements of the soil surrounding liners at different locations before, during, and after tunnel excavation will be also analyzed. The fully coupled three dimensional stress-pore pressure models will be employed by using the commercially available finite element package Abaqus/CAE 2016.HF4.

## **Chapter Two** **Review of Literature**

This chapter briefly reviews the previous studies related to simulation of tunnelling in various regions of the world by using Abaqus and analysis of behaviour of the proposed Baghdad Metro by using different techniques. The theoretical backgrounds for the spatial interpolation techniques and the stress-pore pressure fully coupled formulation are also reviewed in this chapter.

### **2.1 Previous Studies on Simulation of Tunnelling Using Abaqus**

Some of available reviews of simulation of tunnelling using the commercially available finite element package, Abaqus, in various regions of world are presented herein in historical sequence as shown in the following studies:

**Yoo (2005)** presented the results of an investigation on interaction mechanism between tunnelling and ground water using a three dimensional stress-pore pressure coupled finite element model. A parametric study using a three dimensional finite element model was performed on a typical horseshoe shape of tunnel with 10 m diameter and constructed at 25 m below the ground surface in the ground condition frequently encountered in Seoul, Korea. The commercially available finite element package, Abaqus 2002, was used to simulate the sequential tunnelling process by using a fully coupled three dimensional stress-pore pressure finite element model. It was shown that the ground and lining responses were significantly influenced by the relative permeability of the lining, and that the circumferential pre-grouting was an effective means for minimizing the tunnelling and ground water interaction. Also highlighted was the importance of the stress-pore pressure coupled analysis in the numerical prediction of tunnel behaviour. Practical implementations of this study were discussed in great detail.

**Anastasopoulos et al. (2007)** focused on the analysis and design against the longitudinal and lateral vibrations with reference to a proposed immersed tunnel with depth of 70 m in a highly seismic region, in Greece. The multisegment tunnel was modelled as a beam connected to the ground through properly calibrated interaction of springs, dashpots, and sliders. The joints between the tunnel segments were modelled realistically with special nonlinear hyperelastic elements while their longitudinal prestressing due to the great water pressure (7 bar) was also considered. The finite element package, Abaqus 2004, was used to perform nonlinear dynamic transient analysis of the tunnel without ignoring the inertia of the thick walled tunnel, and the influence of segment length and joint properties was investigated parametrically. It was shown that despite ground excitation with acceleration levels exceeding 0.50 g and velocity of about 80 cm/s at the base of the tunnel, net tension and excessive compression between the segments could be avoided with a suitable design of joint gaskets and a selection of relatively small segment lengths. It was concluded that, although this research was prompted by the needs of a specific project, the dynamic analysis methods, the proposed design concepts, and many of the conclusions of the study were sufficiently general and might apply in other immersed tunneling projects.

**Chen and Ruan (2007)** presented the tunnel excavation and lining procedures under high initial stresses and high underground water pressures at Jinping Mountain in China. The Jinping underground hydroelectric power plant is one of major hydropower projects in China. Four high pressure tunnels at about 2000 m depth below JinPing Mountain surface act as waterway towards the power plant. The phreatic water table was located at about 900 m above the tunnels. Coupled hydro-mechanical (HM) behaviour of fractured rock during tunnel excavation was analyzed. The finite element package, Abaqus 6.6, was used to simulate the excavation and lining processes by developing a three dimensional stochastic continuum model that accounted for the heterogeneity of the permeability. The random permeability field was generated using sequential indicator simulations which was mapped into the finite element mesh. The

concrete lining was modelled by shell elements and assumed impervious. Truss elements embedded in a set of three dimensional solid elements were used to model anchors with the embedded element technique. Some simulation results were discussed in details in this study.

**Yoo et al. (2007)** presented the results of three dimensional numerical analysis on the interaction mechanism between tunnelling and ground water in soft ground. A three dimensional stress-pore pressure coupled finite element analysis was conducted on a tunnelling case of the Seoul Metro expansion project in Seoul, Korea, in which the tunnelling caused significant ground water drawdown and associated ground settlements. The subsurface condition for the site under consideration was characterized by multilayers of soil with high ground water table equal to 7 m. The tunnel section considered in this study was approximately 350 m long and consisted of three parallel tunnels with slightly varying elevation. The entire tunnels were excavated through the water-bearing weathered soil deposit. The average cover depth of the tunnels was approximately equal to 20 m. The three tunnel sections had the same cross section (horseshoe) of a maximum height and width of 8.4 m and 11.4 m, respectively, giving a net excavation area of approximately 100 m<sup>2</sup>. The bench cut method was adopted with one segment excavation length of 0.8 m. The commercially available finite element package, Abaqus 2003, was used to simulated the actual tunnelling process consisting of a series of FRP grouting, excavation, and lining installation stages by using Model Change Method where the tunnel was assumed to be fully excavated. The dynamic effect of ground water on the tunnel behaviour and the ground settlements were thoroughly investigated by analyzing the results of analysis. The results highlighted the role of ground water drawdown on the ground settlements and on the tunnel behaviour. Based on the results, the ground surface settlement characteristics associated with ground water drawdown were identified. Practical implications from this study were discussed.

**Yoo and Kim (2008)** presented the results of a numerical investigation of the performance of multifaced tunnelling under a pile-supported building in

water-bearing soft ground. Spatial attention was paid to the effect of tunnelling and ground water interaction on the tunnelling performance. A fully coupled three dimensional stress-pore pressure coupled finite element model was conducted on a tunnelling case of the Seoul Metro expansion project (line-9) in Seoul, Korea. The subsurface condition for the site under consideration was characterized by multilayers of soil with high ground water table of 6 m. The tunnel section considered in this study was horseshoe of a maximum height and width of 8.4 m and 11.7 m, respectively, giving a net excavation area of approximately 87 m<sup>2</sup>. The entire tunnel was excavated through the water-bearing weathered soil deposit. The average cover depth of the tunnel was approximately equal to 17 m. The tunnel was excavated under a three storeys building with a height of 12 m and a clearance of approximately 4 m between pile tip and the tunnel crown. The sidewall drift excavation method was adopted with one round advancement length of 1.0 m. The commercially available finite element package, Abaqus 2007, was used to simulated the actual tunnelling process consisting of a series of FRP grouting, excavation, and lining installation stages by using Model Change Method where the tunnel was assumed to be fully excavated. The results indicated that the ground water drawdown during tunnelling yielded a considerably larger settlement-affected zone than for cases with no ground water drawdown, with a tendency for large portions of ground settlement and ground water drawdown to complete before the tunnel passed a monitoring section. They also revealed that the presence of a building tended to reduce the ground settlements and caused subsurface settlements more or less uniformly with depth. It was shown that lining deformation and its stresses were not significantly affected by the presence of the building for the multifaced tunnelling considered in this study. Axial loads in the piles supporting the building tended to either increase or decrease depending on the pile location relative to the tunnel axis. The patterns of changes in pile axial loads were different from the results of previous studies concerning a single pile.

**Fahimifar and Vakilzadeh (2009)** described briefly the two closed form analytical solutions (Wang's and Penzien' solutions) used for estimating the oval



deformations and forces in circular tunnels due to soil–structure interaction under seismic loading. Then, a comparison between these methods was made by changing the ground parameters. Differences between the results of these two methods in calculating the magnitudes of thrust on tunnel lining were significant. For verifying the results of these two closed form solutions, numerical analyses were performed using finite element code (Abaqus program). These analyses showed that the two closed form solutions provided the same results for full slip condition only.

**Mödlhammer (2010)** discussed different methods to simulate a tunnel drift and the installation of a dual lining system (primary shotcrete shell/secondary cast-in-place concrete inner liner) using the general purpose finite element program Abaqus. The influence of long-time deterioration processes around existing tunnels and its impact on the stability conditions of the combined support system (surrounding ground, shotcrete shell, and inner liner) was also understood. Based on a parameter study, different deterioration processes were simulated coupled with elastic as well as elastoplastic material behaviour. Then, under consideration of the tunnel drift, the interaction between the shotcrete shell and the ground and between the shotcrete shell and the inner liner was also taken into account. The results interpreted the main characteristics of the analyzed deterioration processes on the basis of the obtained stress distributions and displacements of the support elements.

**Namazi et al. (2012)** compared three dimensional finite element modelling of tunnel constructions in stiff soil using nonlinear soil model with low and high  $K_0$  regimes. The Jubilee Line Extension of London's subway consists of the westbound and eastbound twin tunnel's running through the South and East London. The westbound tunnel beneath Street James' Park was re-examined in this study where it was excavated in London Clay using an open-face shield machine with tunnel diameter of 4.75 m and depth approximately of 30.5 m. The commercially available finite element package, Abaqus 6.10, was used to simulate the actual tunnelling process consisting of excavation (deletion of soil

elements inside the tunnel) and lining construction (activation of shell elements around the tunnel) by using Model Change Method. Reduced integration with full Newton solution technique and error-controlled sub-stepping stress point algorithm for solving the nonlinear finite element equations were adopted. The analyses were performed in the undrained conditions. A hydrostatic pore water pressure distribution was defined based on water table 2 m below the ground surface. It was found that modelling using isotropic nonlinear soil with low value of  $K_0$  gave the best matched-fit data on the observed greenfield surface settlement as opposed to the other soil models. In addition, the model was able to replicate the steady state condition of ground movement after the completion of tunnel construction when the tunnel face had passed seven times of the tunnel diameter beyond the boundary point. This steady state condition was not possible to simulate using other soil models.

**Yi et al. (2012)** built a two dimensional numerical simulation using the large finite element analytic software Abaqus at the period of excavation and the initial support in three cross sections located in deeper, shallower, and geological poorer area in order to analyze the deformation law of surrounding rock and support in the process of New Australian Tunnelling Method (NATM) construction. The first stage construction of 215 sections of Dalian Metro in Dalian city, China, was adopted in this study. Three dimensional numerical simulation at different footage excavation size of the same cross section was selected to analyze comparatively the stratum total deformation, the surface deformation, the lining deformation, the lining stress and anchor stress and so on. It showed that the effect of footage was larger and there was a reasonable stage for the primary support of NATM construction.

**Rezaei et al. (2013)** studied the effects of soil stratification and building geometry, position and weight on lining loads. A two dimensional finite element model was applied to simulate the conventional procedure of tunnel excavation and lining using Abaqus software 6.10. The geometry of tunnel, lining segments, injection grout, and around soil properties were adapted from under construction

Tabriz urban railway, Iran, line 2 project. The results showed that ground stratification and building properties (especially the position of buildings) had considerable effects on lining loads.

**Shuaishuai and Yu (2014)** studied the distribution and characteristic of stress and deformation around tunnel rock with and without supporting structure during tunnel excavation through large-scale finite element analysis software Abaqus. It was obtained some useful conclusions which may be helpful for the construction of tunnel.

**Wang et al. (2014)** used the large scale finite element calculation to analyze the settlement deformation caused by shallow buried tunnel construction under complex situations, in order to obtain experiences on design and operation for similar underground engineering. The project of Hefei city plaza tunnel, China, was taken as an example. The finite element package, Abaqus, was used to set three dimensional calculations models to simulate the construction of underground tunnel and to analyze the displacement and stress dynamic response during the construction process. The comparison analysis of the field measurement of the land subsidence was also carried out. The result indicated that the simulation objectively reflected the rules of subsidence during the construction process. Then, evident theory for shallow-buried tunnel construction safely and rapidly was provided.

As a conclusion from the previous mentioned literature review, the stress-pore pressure coupled analysis adopted in this study was adopted by Yoo (2005), Yoo et al. (2007), and Yoo et al. (2008).

## **2.2 Previous Studies on Simulation of The proposed Baghdad Metro**

Some of available studies on the analysis of behaviour of the proposed Baghdad Metro using different techniques are presented herein in historical sequence as shown in the following studies:

**Al- Siaede (1998)** developed analytical models for geotechnical problems around the proposed Baghdad metro basing on mathematical relations. The

ground behaviour modes, effective stress variations, and limits of elastic behaviour for soil surrounding liner as well as the ground surface settlement above tunnels in different soil types for free and compressed air excavation methods respectively were analyzed at nine locations. The results were compared with numerical and monitoring studies in different regions of the world. It was concluded that the analytical techniques adopted in this study gave a practical tool for analysis and predicting ground behaviour during and after tunnel excavation.

**Al-Adili (2002)** used two dimensional models to assess the soil behaviour around liner of the proposed Baghdad metro by using the commercially available finite element package, Plaxis ver.8. The two dimensional finite element models at nine locations (one of these locations is under Tigris) for the proposed Baghdad metro were used to assess the stresses and strains redistribution surrounding the tunnel and ground displacement. The information about the dimensions and the material properties of the concrete tunnel and surrounding soil at those nine locations were obtained from NCCLR. The displacements of the soil clusters and the differential settlements for the foundations of buildings near and above tunnel lining at the locations considered in this study had different rates depending on the soil types and properties, phreatic level, and depth of tunnel. It was noted that the stresses distributions resulted from the tunnel construction at the most locations concentrated around the tunnel liner and beneath foundations of the buildings. It was concluded that the proposed Baghdad metro at the locations selected in this study had no serious problems in settlements and deformations with respect to the tunnel boring method.

**Salim (2006)** used the finite element method to analyze the behaviour of tunnels in clay soils. Time independent analyses were used to represent the excavation stage and time dependent analyses were used to represent the behaviour of the unlined tunnel after a long time. Typical location of the proposed Baghdad metro was considered as a basic problem where one route only was assumed at this location. It was assumed circular cross section of this tunnel with outer diameter of 5.9 m and concrete liner thickness of 0.45 m. It was also

assumed that the tunnel axis at a depth of 18 m below the ground surface. The subsurface condition for this site was assumed consisting of fully saturated multilayers of soil. The first, second, and third layers were assumed as silty clay, sand to silty sand, and sand layer respectively. The entire tunnel was assumed excavated through the second layer. The finite element program "Modf-CRISP" was used to analyze the effects of tunnelling this metro at this typical location on the vertical and horizontal effective stresses and the excess pore water pressure formation and dissipation. It was concluded that the change in diameter and depth of the tunnel had a significant effect on the vertical and horizontal stresses and the excess pore water pressure. The maximum surface settlement using consolidation analysis was approximately twice that using undrained analysis. The propagation of plastic zone was extent to the surface as the tunnel diameter increases and the depth of the tunnel decreases. Most of the strains occurred near the tunnel opening. The magnitude and pattern of the vertical and horizontal strains were very similar but with opposite signs. Finally, some equations were derived from those results to reduce the risk of damages occurring due to tunnelling from which the prediction of the settlement trough width, maximum settlement, and radius of the plastic zone around the tunnel could be estimated.

**Fattah et al. (2012)** investigated the validity of transmitting boundaries in dynamic analysis of soil structure interaction problems. As a case study, the proposed Baghdad metro line was considered. The information about the dimensions and the material properties of the concrete tunnel and surrounding soil were obtained from Salim's study in 2006. A parametric study was carried out to investigate the effect of several parameters including the peak value of the horizontal component of earthquake displacement records and the frequency of the dynamic load. The computer program "Mod-MIXDYN" was used for the analysis. The numerical results were analyzed for three conditions; finite boundaries (traditional boundaries), infinite boundaries modelled by infinite elements (5 nodes mapped infinite element) presented by Selvadurai and Karpurapu in 1988, and infinite boundaries modelled by dashpot elements

(viscous boundaries). It was found that the transmitting boundary absorbed most of the incident energy. The distinct reflections observed in the "fixed boundaries" case disappeared in the "transmitted boundaries" case. This was true for both cases of using viscous boundaries or mapped infinite elements. The type and location of the dynamic load were the two controlling factors in deciding the importance of using infinite boundaries. It was found that the results were greatly influenced when the earthquake was applied as a base motion or the pressure load was applied at the surface ground. The horizontal displacement on the free surface increased significantly for infinite boundaries and it increased about 7.0 times the value of using finite elements only.

**Shlash et al. (2014)** discussed the stresses around a tunnel during construction stages. The finite element method was adopted as an effective approach to analyze the problem using "SIGMA/W" program. The proposed Baghdad metro at Bab Al-Muaddam substation was considered as a basic problem where one route only was assumed at this location. It was assumed circular cross section of this tunnel with outer diameter of 10 m and concrete liner thickness of 0.25 m. It was also assumed that the tunnel axis at a depth of 15 m below the ground surface. The subsurface condition for this site was assumed consisting of one fully saturated layer of C- $\phi$  soil. Excavation of tunnel section was assumed to carry out through six stages. These stages include excavation of each stage and lining it. The research included the study of the behaviour of soil due to excavation of tunnel by calculating the displacements and stresses in three positions of tunnel (crown, wall, and invert) during the various stages of construction. The finite element analyses were carried out using elastoplastic and linear elastic models for the soil and the concrete liner respectively. It was found that increasing the number of excavation stages of section decreased the displacement comparing with excavation using one stage.

As a conclusion from the previous mentioned literature review, there is some lack in studies that were conducted to relate the actual soil strata and their properties and the actual depth of water table. It is also concluded that the

mechanical and hydrological interaction between the tunnelling and ground water was not realistically captured. The stress-pore pressure coupled analysis adopted in this study was not adopted in those studies.

### **2.3 Spatial Interpolation Techniques**

Most interpolation methods can be divided into two main types called global and local. Global interpolators use all the available data to provide estimates for the points with unknown values; local interpolators use only the information in the vicinity of the point being estimated. Global interpolators are often used to remove the effects of major trends before using local interpolators to analyze the residuals. Kriging is a particular type of local interpolation using more advanced geostatistical techniques (Burrough, 1986).

Interpolation methods may also be classified as exact or inexact. Using exact interpolation, the predicted values at the points for which the data values are known will be the known values; inexact interpolation methods remove this constraint (i.e. the observed data values and the interpolated values for a given point are not necessarily the same). Inexact interpolation may produce a smoother (and arguably more plausible) surface (Burrough, 1986).

Interpolation methods may be either deterministic or stochastic. Deterministic methods provide no indication of the extent of possible errors, whereas stochastic methods provide probabilistic estimates (Burrough and McDonnell, 1998).

There are two broad approaches to the global interpolation. One uses classification techniques to infer the values of one variable attribute based upon a knowledge of the values of another attribute. The other uses regression techniques to infer the value of the variable of interest based upon a knowledge of attributes that are easy to measure. The classification techniques may be used if spatial data are very sparse, although the regression techniques would generally be preferred if there is sufficient data. The classification techniques are global, inexact, and

deterministic while the regression techniques are global, inexact, and stochastic (Burrough and McDonnell, 1998).

In recent years, GIS capabilities for spatial interpolation have improved by integration of advanced methods within GIS as well as by linking GIS to systems designed for modelling, analysis, and visualization of continuous fields.

In this study, five interpolation methods provided in the ArcGIS 10.5 are used with the best options available for each method to generate different spatial raster surfaces for ground surface elevations and different spatial raster surfaces for ground water levels. Then, best of the best spatial raster surfaces for ground surface elevations generated from ground surface elevations recorded at wells in Baghdad Governorate and Baghdad City and best of the best spatial raster surfaces for static water levels generated from static water levels observed at wells in Baghdad Governorate and Baghdad City are depended to determine the water table depths on the proposed Baghdad Metro. These interpolation methods are Inverse Distance Weight (IDW), Natural Neighbour (NN), Spline, Trend, and Kriging.

## 2.4 Stress-Pore Pressure Coupled Analysis

In order to realistically capture the interaction mechanism between the tunnelling and ground water, a three dimensional stress-pore pressure fully coupled formulation is preferably to be adopted. A commercially available finite element package, Abaqus, is capable of simulating the stress-strain-strength behaviour of ground in stress-pore pressure fully coupled manner.

In Abaqus, a porous medium is approximately modelled by attaching the finite element mesh to the solid phase. Liquid can flow through this mesh. Equilibrium is expressed by writing the principle of virtual work for the volume (V) under consideration in its current configuration at time  $t$  (Abaqus Inc., 2016):

$$\int_V \sigma : \delta \varepsilon dV = \int_S t \cdot \delta v dS + \int_V \hat{f} \cdot \delta v dV, \dots\dots\dots(2-1)$$



where  $\delta v$  is a virtual velocity field,  $\delta \epsilon$  is the virtual rate of deformation,  $\sigma$  is the true (Cauchy) stress,  $t$  is the surface tractions per unit area,  $\hat{f}$  is the body forces per unit volume, and  $S$  is the surface under consideration.

For the stress-pore pressure coupled analysis,  $\hat{f}$  includes the weight of the wetting liquid ( $f_w$ ) which is defined as follows:

$$f_w = (sn + n_t) \rho_w g, \dots\dots\dots(2-2)$$

where  $s$  is the degree of saturation,  $n$  is the porosity,  $n_t$  is the volume of trapped wetting liquid per unit of current volume,  $\rho_w$  is the unit weight of water, and  $g$  is the gravitational acceleration which it is assumed to be constant and in a constant direction.

For simplicity it is considered this loading ( $f_w$ ) explicitly so that any other gravitational term in  $\hat{f}$  is associated only with the weight of the dry porous medium. Thus, Equation 2-1 can be written as follows:

$$\int_v \sigma : \delta \epsilon dV = \int_S t \cdot \delta v dS + \int_v f \cdot \delta v dV + \int_v (sn + n_t) \rho_w g \cdot \delta v dV, \dots\dots\dots(2-3)$$

where  $f$  are all body forces except the weight of the wetting liquid.

In a finite element model, equilibrium (Equation 2-3) is approximated as a finite set of equations by introducing interpolation functions. The interpolation is assumed to be based on material coordinates in the material skeleton (a “Lagrangian” formulation).

As mentioned for the equilibrium equation (Equation 2-1), the liquid can flow through the finite element mesh. Therefore, a continuity equation is required for the liquid, equating the rate of increase in liquid mass stored at a point to the rate of mass of liquid flowing into the point within the time increment. This continuity statement is written in a variational form as a basis for finite element approximation. Darcy's law or, alternatively, Forchheimer's law is used to described the constitutive behaviour for pore-fluid flow. Darcy's law is generally applicable to low fluid flow velocities whereas Forchheimer's law is commonly used for situation involving higher flow velocities. Darcy's law ca be thought of as a linearized version of Forchheimer's law. Darcy's law states that, under

uniform conditions, the volumetric flow rate of the wetting liquid through a unit area of the medium is proportional to the negative of the gradient of the piezometric head as shown in the following equation (Bear, 1972):

$$sn v_w = -\hat{k} \cdot \frac{\partial \Phi}{\partial x}, \dots\dots\dots(2-4)$$

where  $sn v_w$  is the volumetric flow rate of the wetting liquid through a unit area of the medium, where  $v_w$  is the velocity of the wetting liquid,  $\hat{k}$  is the permeability of the medium,  $\Phi$  is the piezometric head, and  $x$  is the unit vector in x-direction. In Abaqus formulation,  $\hat{k}$  depends on the saturation of the phase being considered and the porosity of the medium as follows:

$$\hat{k} = k_s \hat{k}, \dots\dots\dots(2-5)$$

where  $k_s(s)$  provides the dependency on saturation, with  $k_s(1)$  equal to one and  $k$  ( $x, e$ ) is the permeability of the fully saturated medium (where  $e$  is the void ratio of the medium). In Abaqus,  $k_s(s)$  is defined as suggested by Nguyen and Durso (1983) as follows:

$$k_s = s^3, \dots\dots\dots(2-6)$$

The continuity equation is satisfied approximately in the finite element model by using excess wetting liquid pressure as the nodal variable (degree of freedom 8) interpolated over the elements. It is defined as follows:

$$\int_v \left( \delta u_w \left\{ \frac{\rho_w}{\rho_w^o} (sn + n_r) - \frac{1}{J} \left[ \frac{\rho_w}{\rho_w^o} (sn + n_r) \right] \right\} - \Delta t \frac{\rho_w}{\rho_w^o} sn \frac{\partial \delta u_w}{\partial x} \cdot v_w \right) dV + \Delta t \int_s \delta u_w \frac{\rho_w}{\rho_w^o} snn \cdot v_w dV = 0, \dots\dots\dots(2-7)$$

where  $\rho_w^o$  is the density of the liquid in the reference configuration;  $\delta u_w$  is an arbitrary, continuous, variation field,  $J$  is the ratio of the medium volume in the current configuration ( $dV$ ) to its volume in the reference configuration ( $dV_o$ ).

The continuity equation (Equation 2-7) is satisfied approximately in the finite element model by using excess wetting liquid pressure as the nodal variable (degree of freedom 8) interpolated over the elements.

The backward Euler approximation is used to integrate Equation 2-7 over time. Then, the total derivative of this integrated variational statement of continuity with respect to the nodal variables is required for the Newton iterations which are used to solve the nonlinear, coupled, equilibrium and continuity equations (Equation 2-3 and 2-7).

## **Chapter Three**

### **Description of The Proposed Baghdad Metro**

This chapter includes description of the layout of the proposed Baghdad metro. It also views the data of wells for Baghdad Governorate and Baghdad City which are used to generate different spatial raster surfaces for ground surface elevations and static water levels to compute the water table depths at different locations for the proposed Baghdad metro form best of the best spatial raster surfaces for ground surface elevations and static water levels. Then, details of geometry and depth of this metro at these locations are shown and soil strata with their properties for each one are also given.

#### **3.1 Layout and Geometry of The Proposed Baghdad Metro**

Baghdad Governorate lies in the middle of Iraq within the Mesopotamians Plain. It is the capital of Iraq. The capital city for Baghdad Governorate is Baghdad City. Six governorates surround Baghdad Governorate. These governorates are: Babylon, Wasit, Diyala, Salah Al-Din, Karbala'a, and Anbar as shown in Figure 3.1.



**Figure 3.1: Iraqi map showing Baghdad and adjacent governorates.**

One of the two main rivers of Iraq, Tigris, passes through Baghdad Governorate. The another river, Euphrates, borders Baghdad Governorate at the southwest as shown in Figure 3.2. The main source of Baghdad Governorate is Tigris River.

Tigris River passes through Baghdad City dividing it to two parts; Karkh on the west of river and Rasafa on the east of river. Baghdad City is bounded from the east by Diyala river which joins Tigris river at the southeast of Baghdad City. The Army Canal, 24 km long, recharges from Tigris river in the northern part of Baghdad City and terminates in the southern part of Diyala river (Al-Hiti, 1985). The satellite image (Landsat) of Baghdad City with 60 cm error plotting on it the information mentioned above is shown in Figure 3.3.

Baghdad City was built on the Tigris flood plain sediments of Recent Pleistocene period. Below the top layer of artificial sediment (or fill) brought about by renewing constructions in and around the Baghdad, starts the flood plain natural sediments. There are composed of a sequence of silty clays, silts, and sands with some gravelly horizons. These sediments replace themselves horizontally and vertically (Al-Basrawi et al., 2015).

The proposed Baghdad metro lies in Baghdad City. It has total length equal to 39 km including 42 stations. This proposed project comprises two lines that connect both sides of Baghdad City; Karkh and Rasafa. The central station in which the two lines of Baghdad metro encounter each other lies in Rasafa at Killani Square on the Jamhurriya street as shown in Figure 3.4.

**Table C.35: Initial conditions of pore water pressures and effective stresses of the three dimensional finite element model of location-18/line-2, with referencing to Table B.35.**

Layer no.		Pore pressure (kN/m <sup>2</sup> )		Effective stress (kN/m <sup>2</sup> )		Lateral coefficient (K <sub>a</sub> )
		Top	Bottom	Top	Bottom	
Above W.T.	1	0.000		0.000	14.880	0.983
	2			14.880	47.432	0.933
Below W.T.	2	0.000	24.200	47.432	70.059	0.933
	3	24.200	89.200	70.059	130.184	0.729
	4	89.200	174.200	130.184	209.659	0.933
	5	174.200	232.300	209.659	282.284	0.171

**Table C.36: Initial conditions of pore water pressures and effective stresses of the three dimensional finite element model of location-19/line-2, with referencing to Table B.36.**

Layer no.		Pore pressure (kN/m <sup>2</sup> )		Effective stress (kN/m <sup>2</sup> )		Lateral coefficient (K <sub>a</sub> )
		Top	Bottom	Top	Bottom	
Above W.T.	1	0.000		0.000	29.760	0.983
	2			29.760	51.827	0.933
Below W.T.	2	0.000	115.900	51.827	160.193	0.933
	3	115.900	287.800	160.193	375.068	0.171

**Table C.37: Initial conditions of pore water pressures and effective stresses of the three dimensional finite element model of location-20/line-2, with referencing to Table B.37.**

Layer no.		Pore pressure (kN/m <sup>2</sup> )		Effective stress (kN/m <sup>2</sup> )		Lateral coefficient (K <sub>a</sub> )
		Top	Bottom	Top	Bottom	
Above W.T.	1	0.000		0.000	21.655	0.933
Below W.T.	1	0.000	15.800	21.655	36.349	0.933
	2	15.800	29.800	36.349	49.789	1.000
	3	29.800	58.800	49.789	77.484	1.000
	4	58.800	98.800	77.484	121.484	0.589
	5	98.800	119.800	121.484	152.984	0.271
	6	119.800	304.100	152.984	355.714	0.589

## Appendix D

### Change Curves of The Vertical Displacements (U3) of The Front Crown and Invert Points During and After Tunnel Excavation for 37 Locations on The Proposed Baghdad Metro

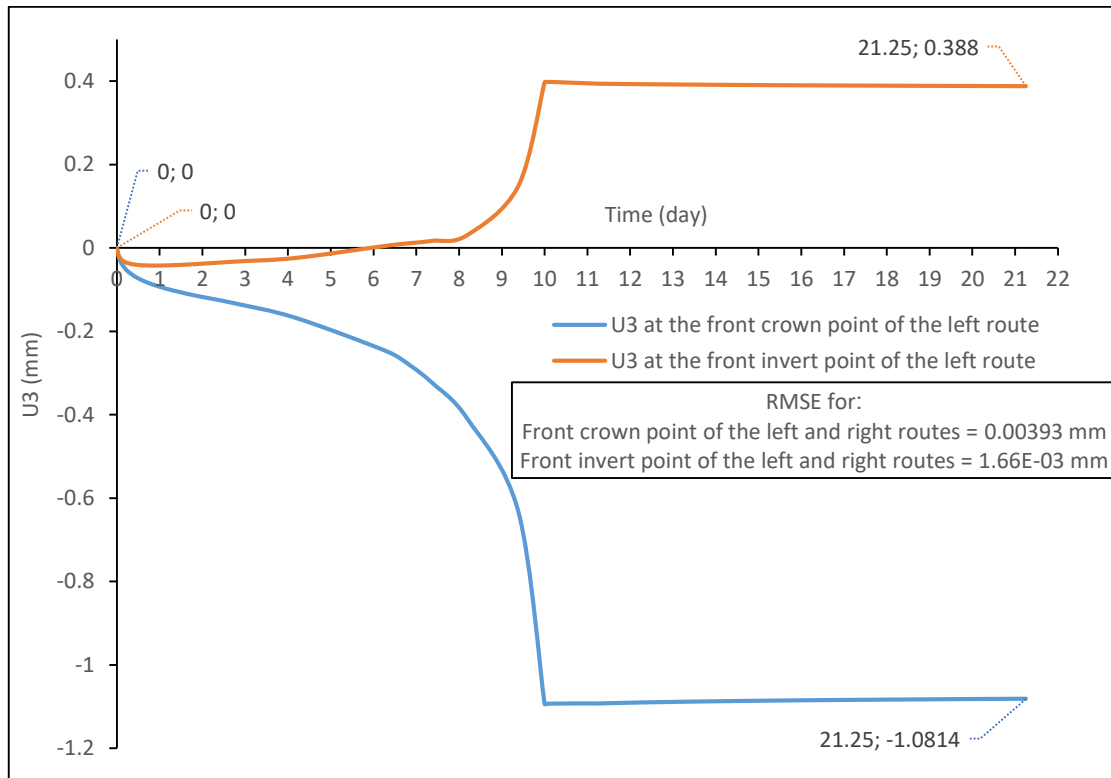


**Figure D.1: Change curves of the vertical displacements (U3) for the front faces of the left and right routes at location-2/line-1 during excavation (10 days), linings installation (30 hours), and consolidation (10 days) steps.**

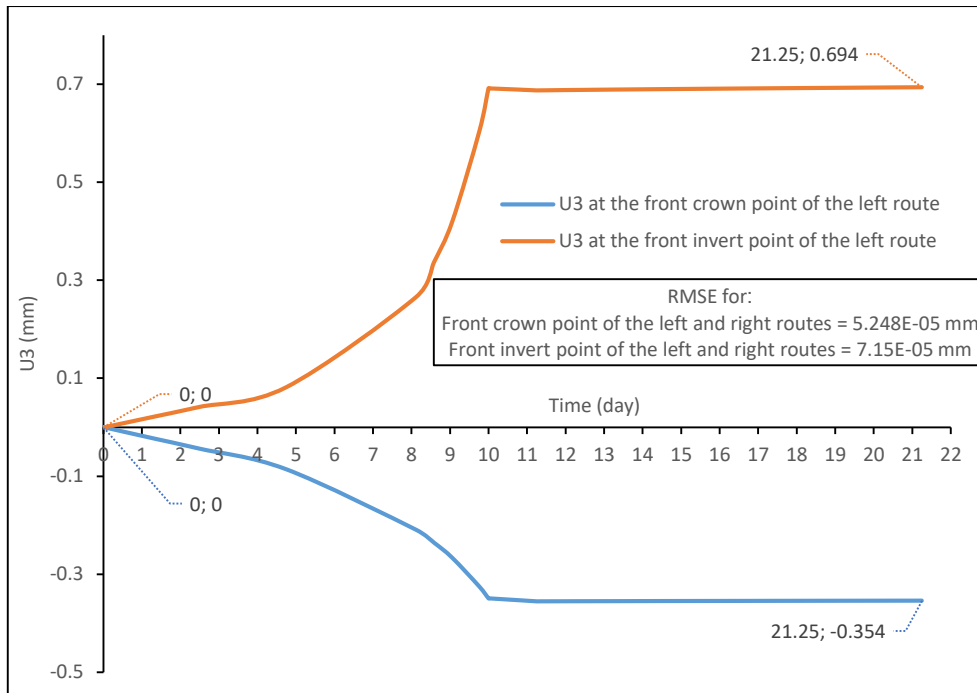


**Figure D.2: Change curves of the vertical displacements (U3) for the front faces of the left and right routes at location-3/line-1 during excavation (10 days), linings installation (30 hours), and consolidation (10 days) steps.**

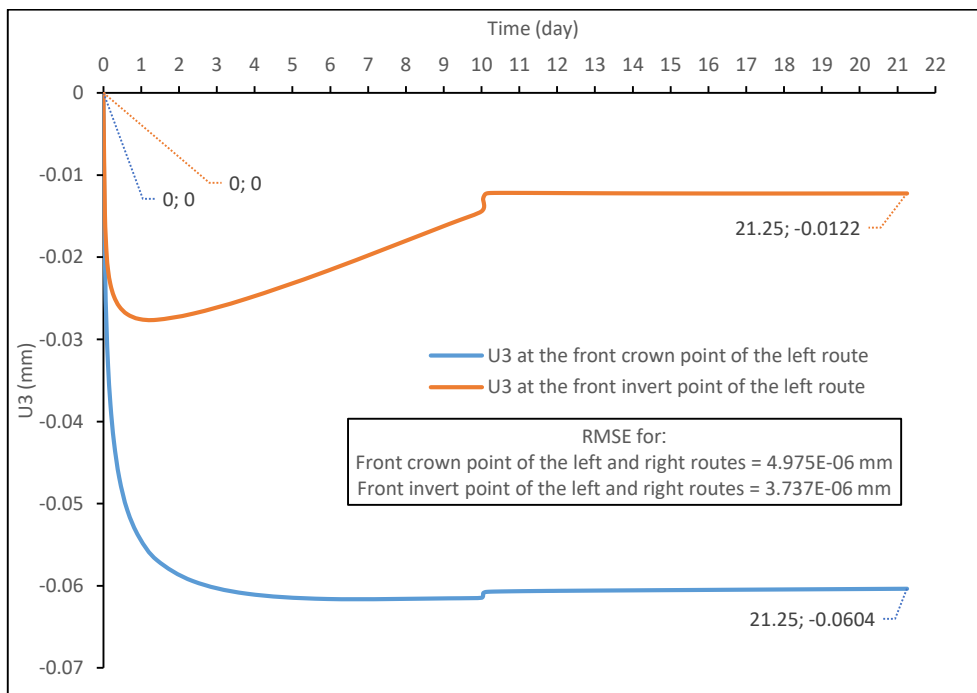


**Figure D.3: Change curves of the vertical displacements (U3) for the front faces of the left and right routes at location-4/line-1 during excavation (10 days), linings installation (30 hours), and consolidation (10 days) steps.**



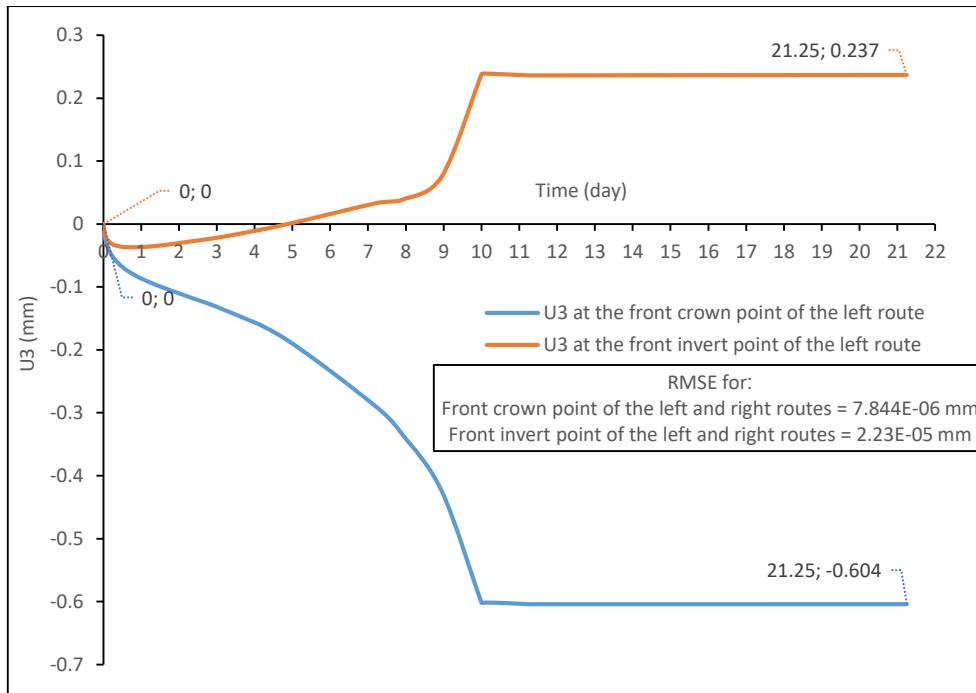


**Figure D.4: Change curves of the vertical displacements (U3) for the front faces of the left and right routes at location-5/line-1 during excavation (10 days), linings installation (30 hours), and consolidation (10 days) steps.**

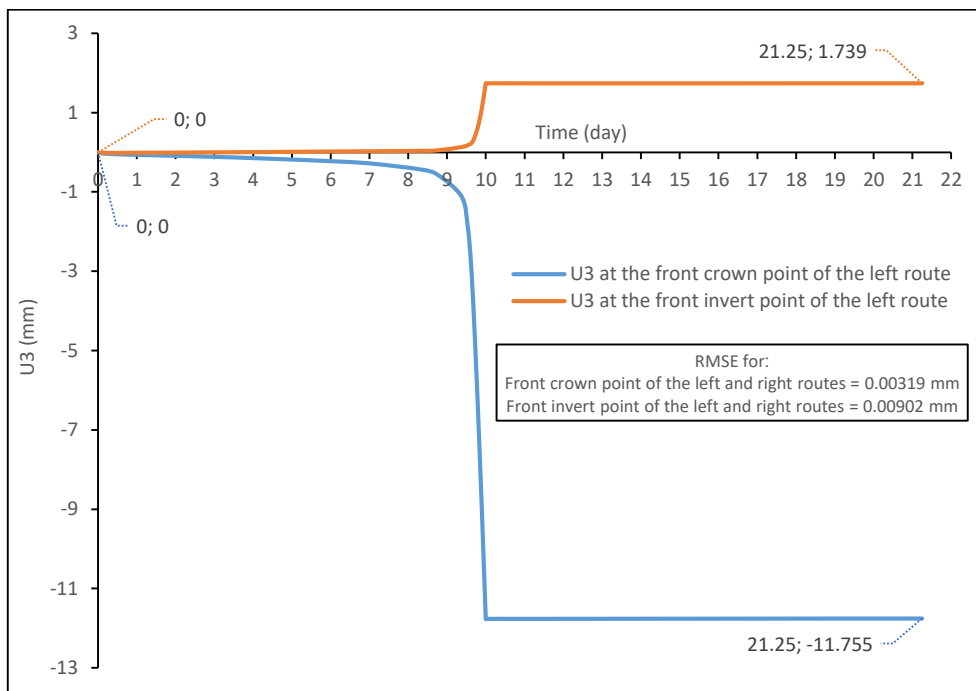


**Figure D.5: Change curves of the vertical displacements (U3) for the front faces of the left and right routes at location-6/line-1 during excavation (10 days), linings installation (30 hours), and consolidation (10 days) steps.**

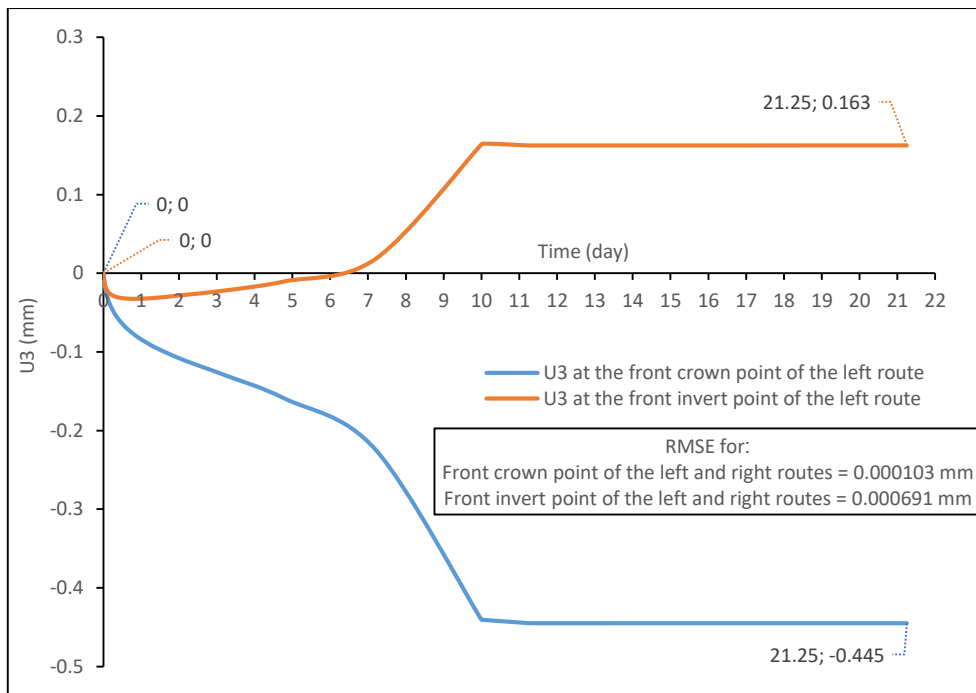


**Figure D.6: Change curves of the vertical displacements (U3) for the front faces of the left and right routes at location-7/line-1 during excavation (10 days), linings installation (30 hours), and consolidation (10 days) steps.**

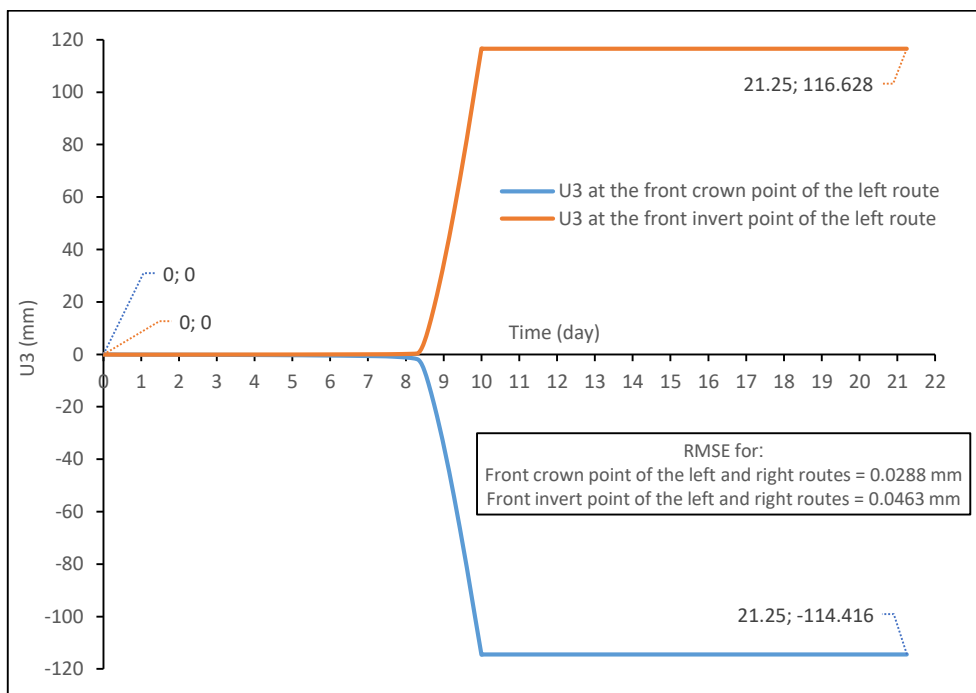


**Figure D.7: Change curves of the vertical displacements (U3) for the front faces of the left and right routes at location-8/line-1 during excavation (10 days), linings installation (30 hours), and consolidation (10 days) steps.**

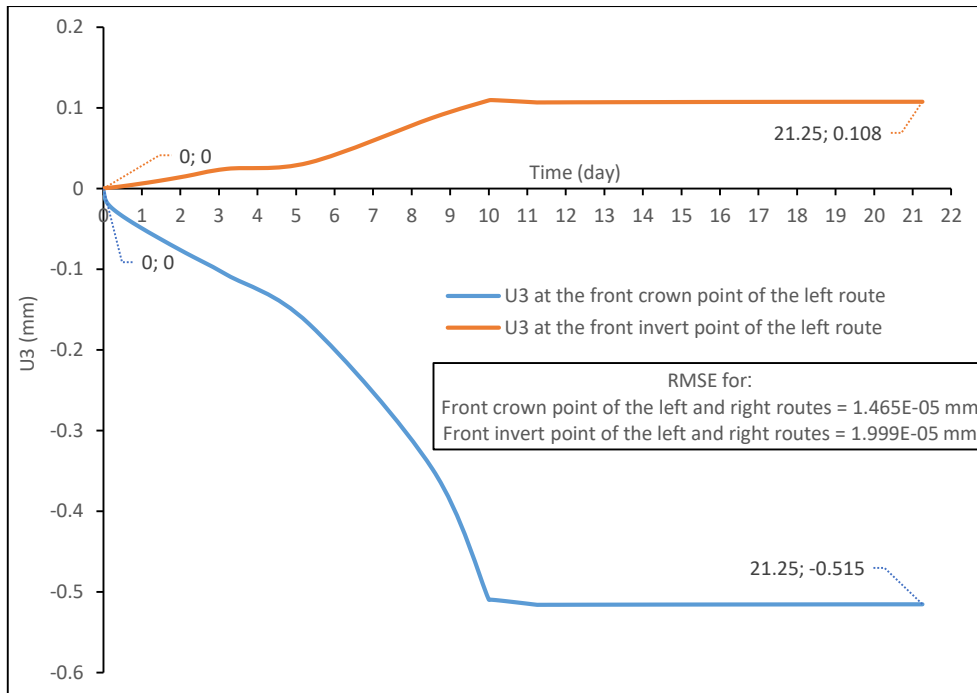


**Figure D.8: Change curves of the vertical displacements (U3) for the front faces of the left and right routes at location-9/line-1 during excavation (10 days), linings installation (30 hours), and consolidation (10 days) steps.**

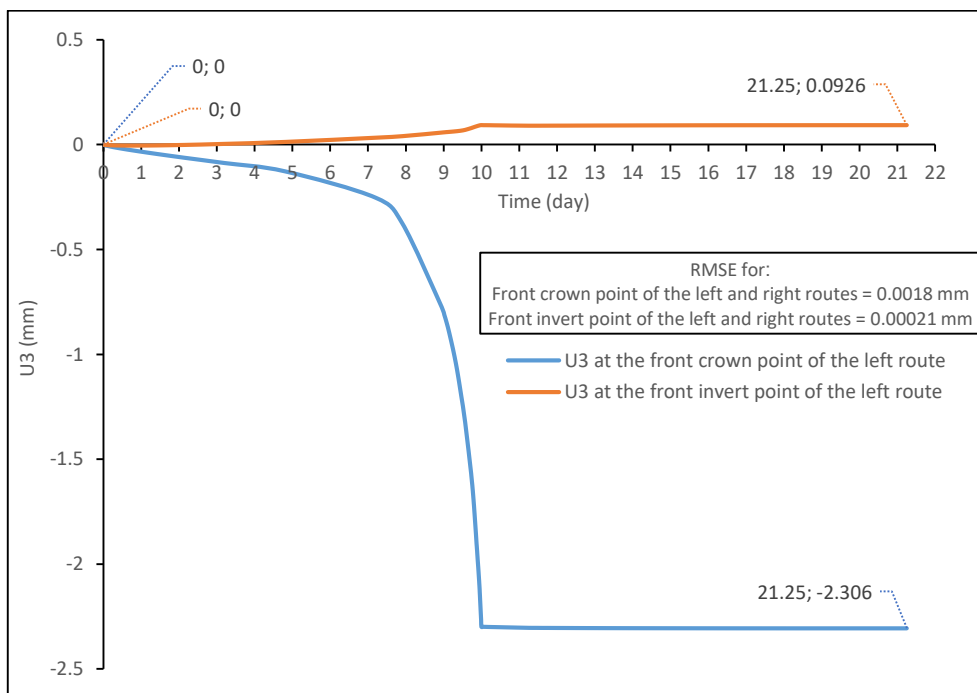


**Figure D.9: Change curves of the vertical displacements (U3) for the front faces of the left and right routes at location-10/line-1 during excavation (10 days), linings installation (30 hours), and consolidation (10 days) steps.**

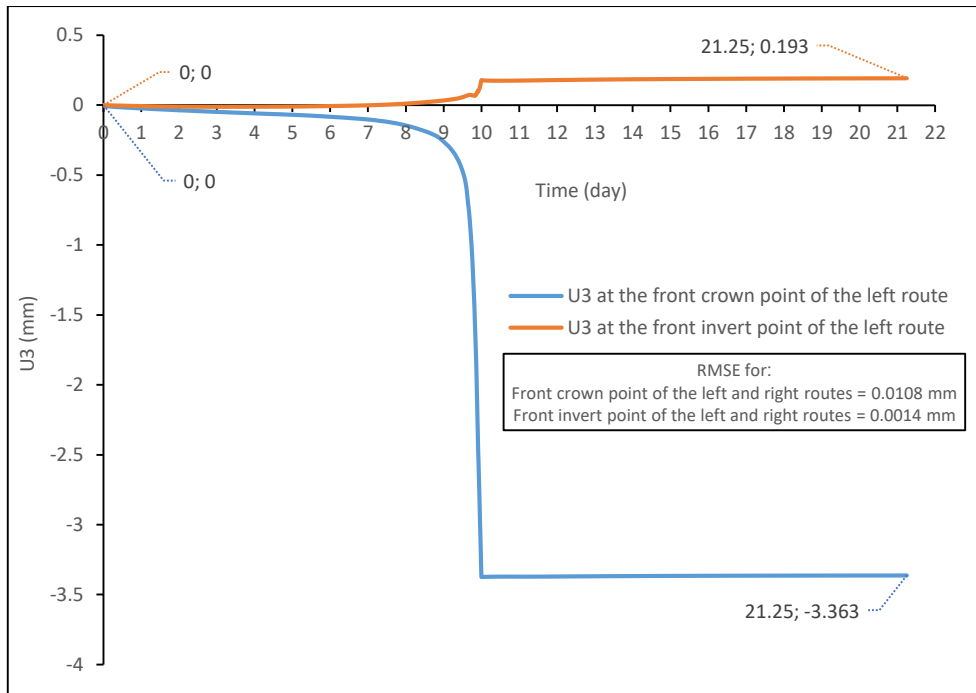


**Figure D.10: Change curves of the vertical displacements (U3) for the front faces of the left and right routes at location-11/line-1 during excavation (10 days), linings installation (30 hours), and consolidation (10 days) steps.**

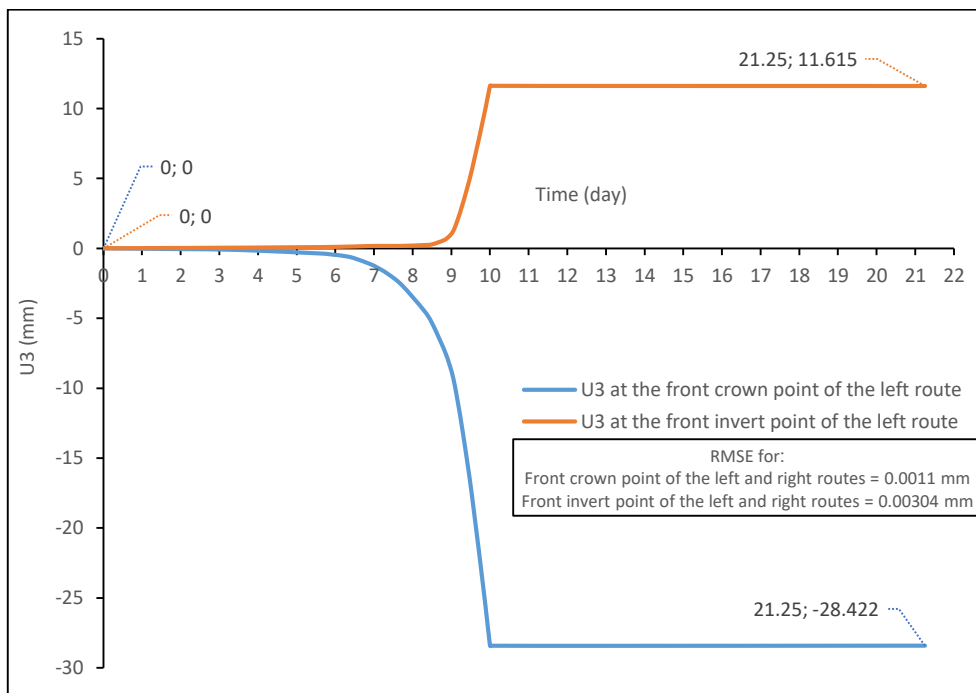


**Figure D.11: Change curves of the vertical displacements (U3) for the front faces of the left and right routes at location-12/line-1 during excavation (10 days), linings installation (30 hours), and consolidation (10 days) steps.**

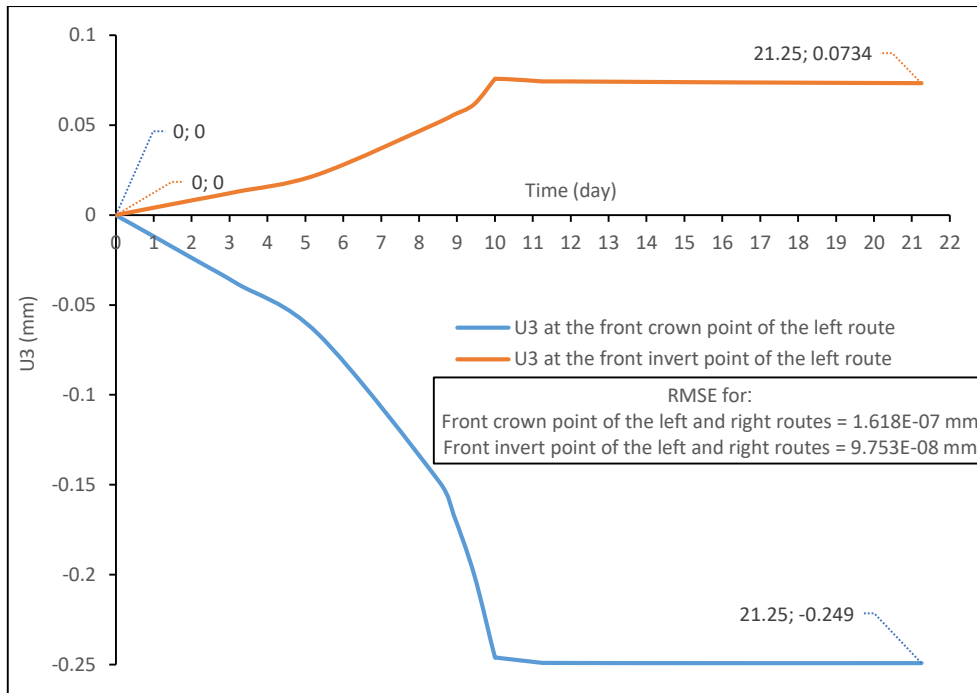


**Figure D.12: Change curves of the vertical displacements (U3) for the front faces of the left and right routes at location-13/line-1 during excavation (10 days), linings installation (30 hours), and consolidation (10 days) steps.**

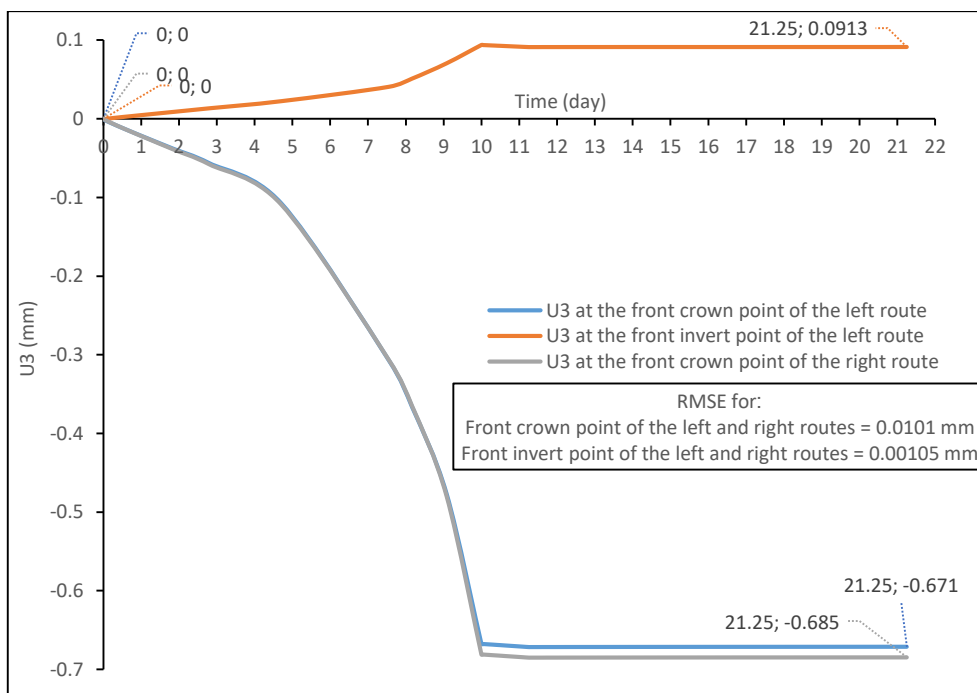


**Figure D.13: Change curves of the vertical displacements (U3) for the front faces of the left and right routes at location-14/line-1 during excavation (10 days), linings installation (30 hours), and consolidation (10 days) steps.**

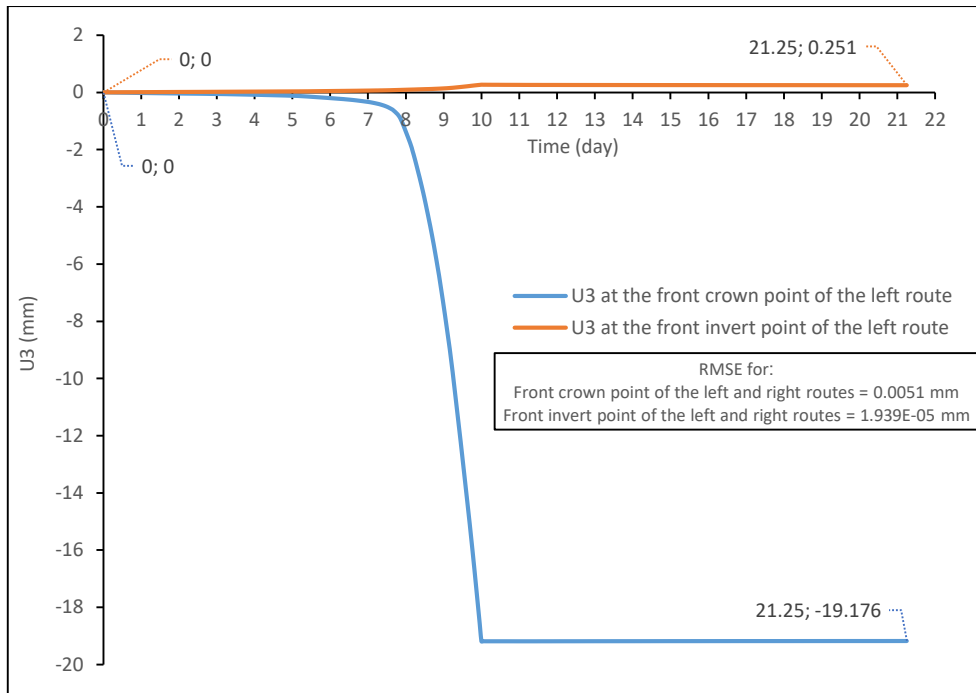
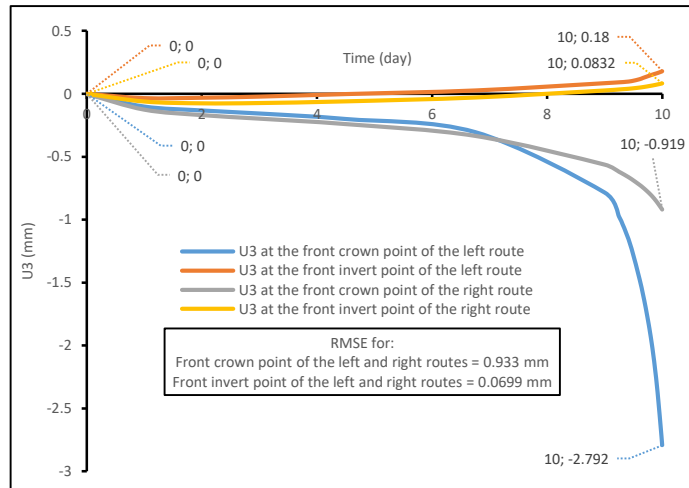
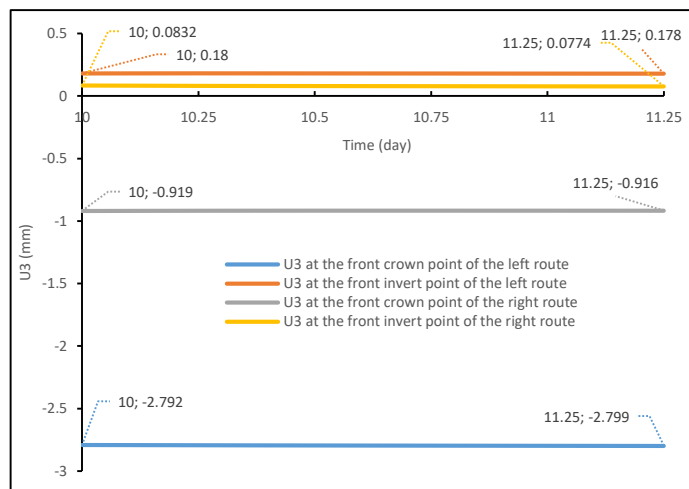


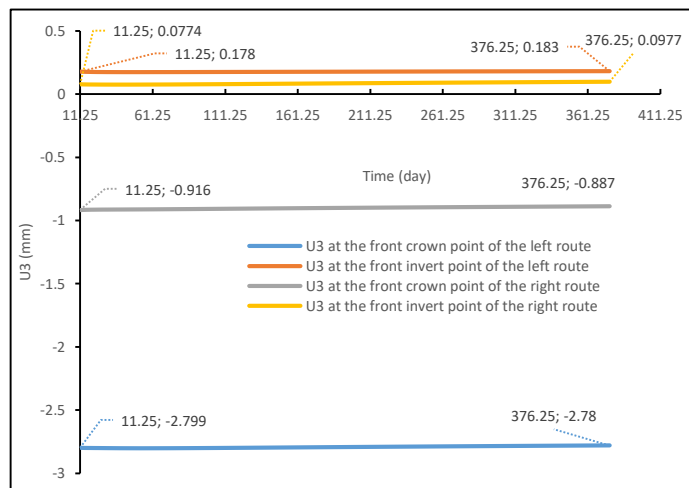
**Figure D.14: Change curves of the vertical displacements (U3) for the front faces of the left and right routes at location-15/line-1 during excavation (10 days), linings installation (30 hours), and consolidation (10 days) steps.**



**(A) Excavation step (10 days)**



**(B) Linings installation step (30 hours; 1.25 days)**



**(C) Consolidation step (1 year)**

**Figure D.15: Change curves of the vertical displacements (U3) for the front faces of the left and right routes at location-16/line-1 during excavation (10 days), linings installation (30 hours), and consolidation (1 year) steps.**

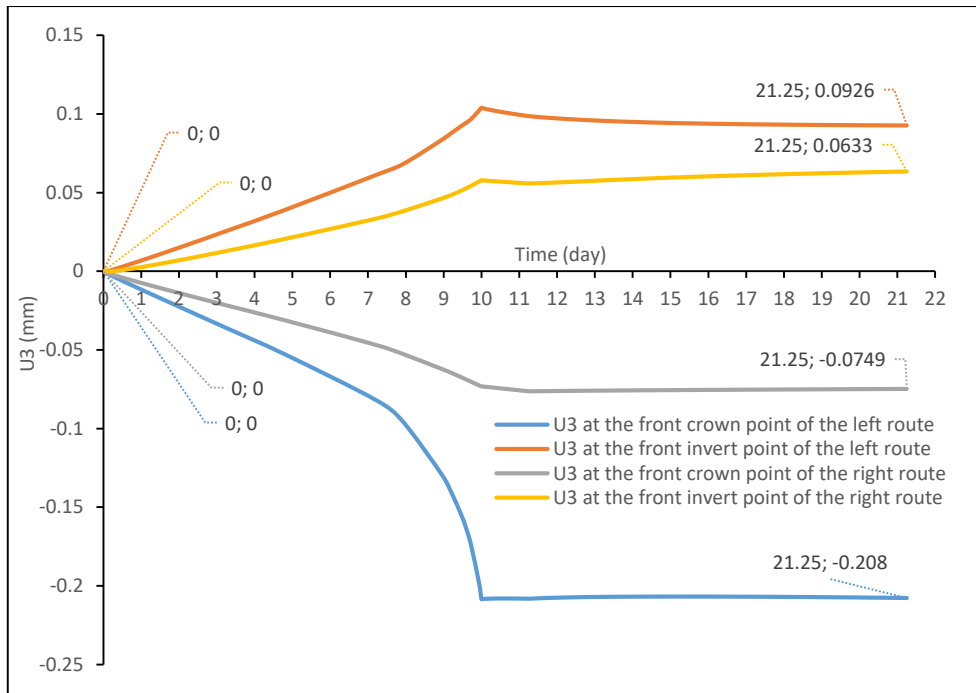


**Figure D.16: Change curves of the vertical displacements (U3) for the front faces of the left and right routes at location-17/line-1 during excavation (10 days), linings installation (30 hours), and consolidation (10 days) steps.**

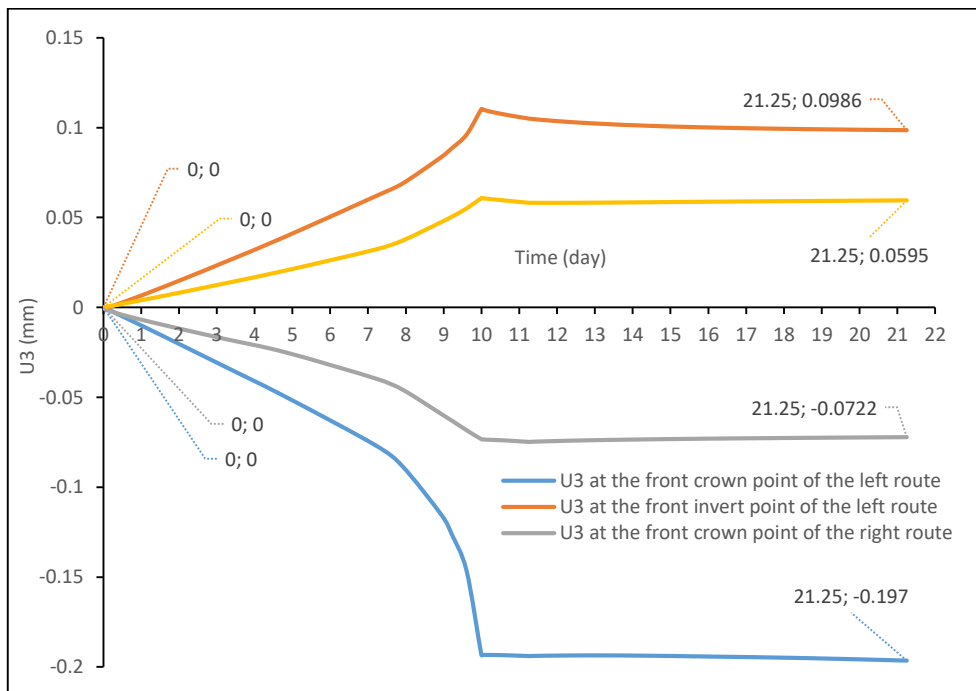


**Figure D.17: Change curves of the vertical displacements (U3) for the front faces of the left and right routes at location-18/line-1 during excavation (10 days), linings installation (30 hours), and consolidation (10 days) steps.**



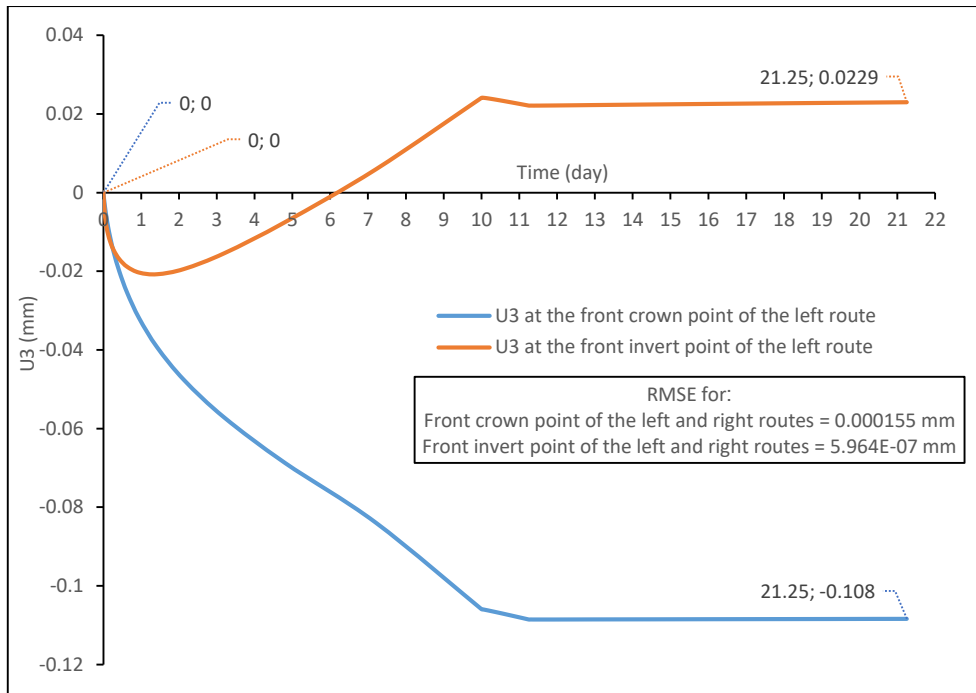


**Figure D.18: Change curves of the vertical displacements (U3) for the front faces of the left and right routes at location-1/line-2 during excavation (10 days), linings installation (30 hours), and consolidation (10 days) steps.**

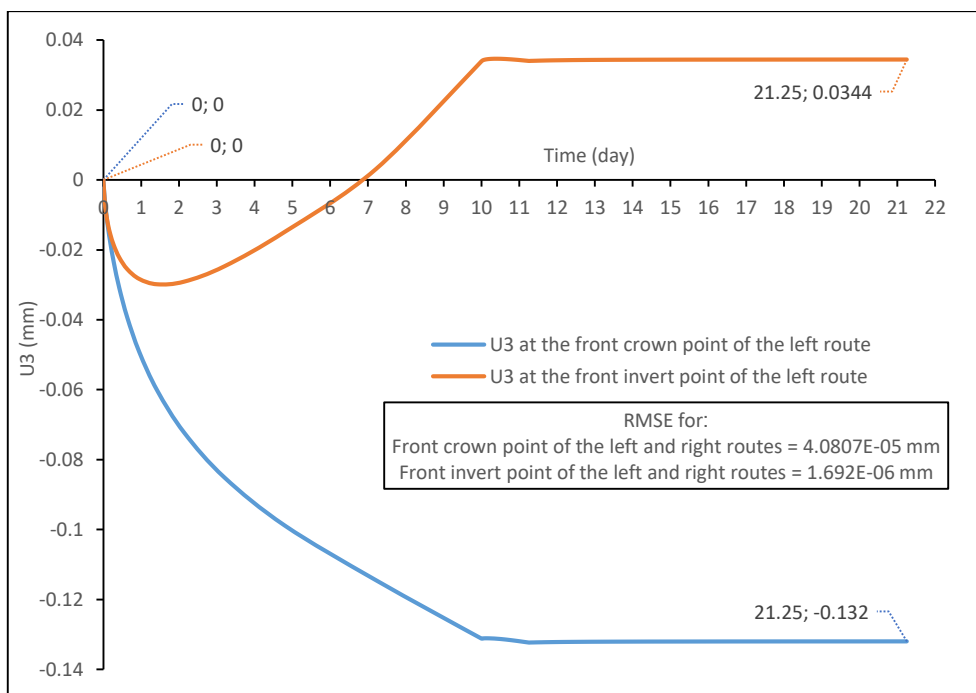


**Figure D.19: Change curves of the vertical displacements (U3) for the front faces of the left and right routes at location-2/line-2 during excavation (10 days), linings installation (30 hours), and consolidation (10 days) steps.**

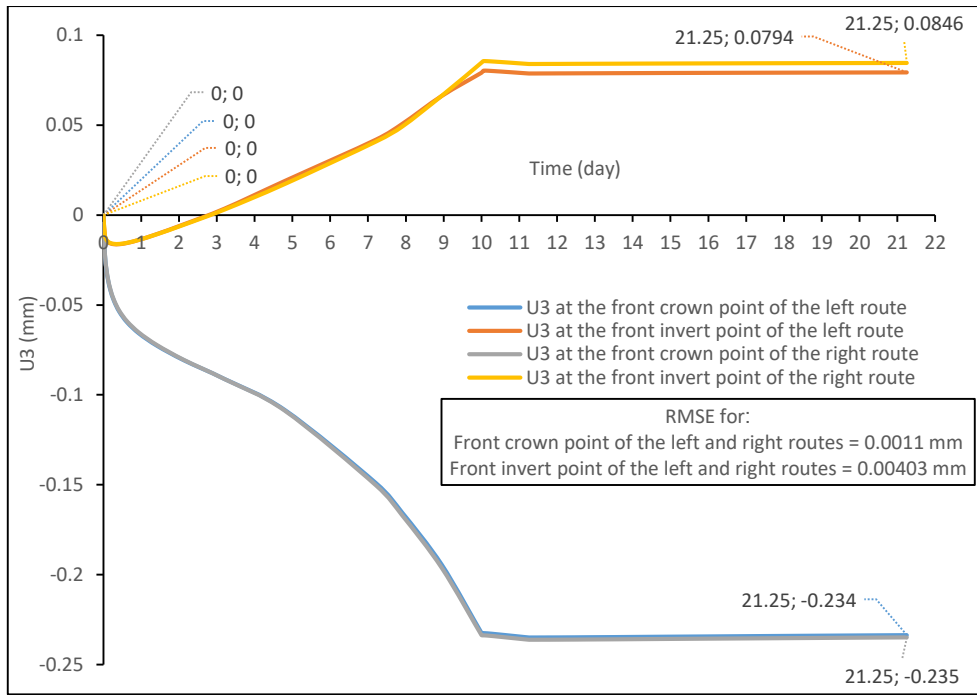


**Figure D.20: Change curves of the vertical displacements (U3) for the front faces of the left and right routes at location-3/line-2 during excavation (10 days), linings installation (30 hours), and consolidation (10 days) steps.**

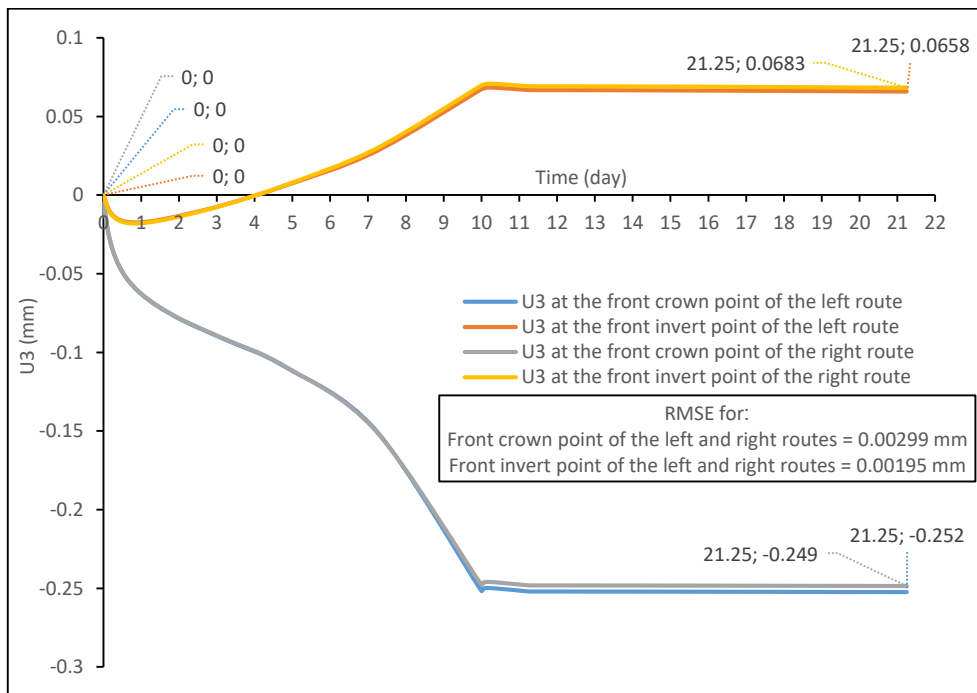


**Figure D.21: Change curves of the vertical displacements (U3) for the front faces of the left and right routes at location-4/line-2 during excavation (10 days), linings installation (30 hours), and consolidation (10 days) steps.**

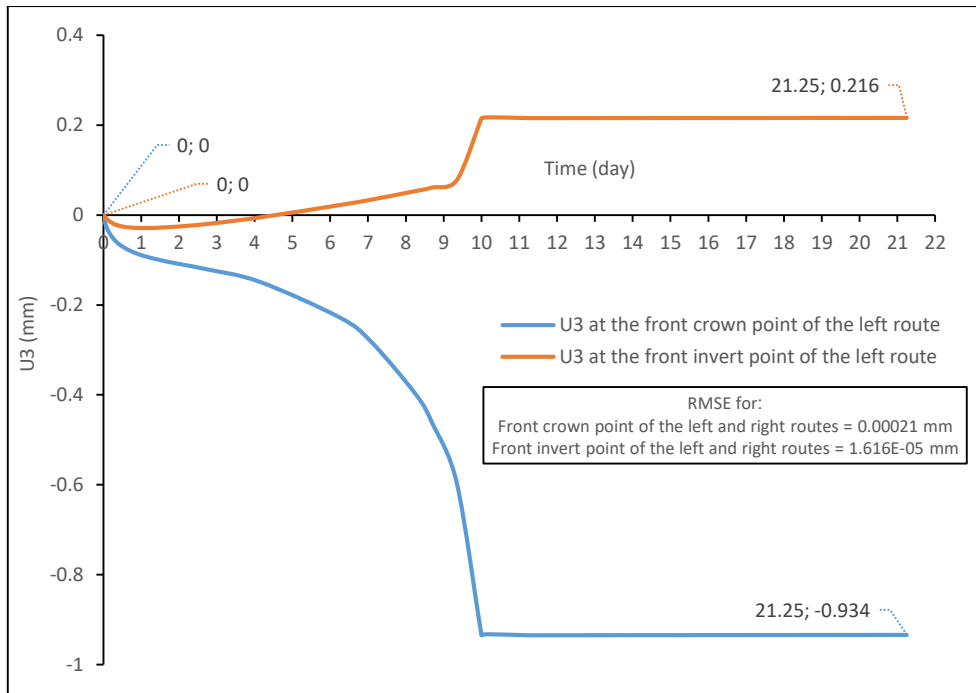


**Figure D.22: Change curves of the vertical displacements (U3) for the front faces of the left and right routes at location-5/line-2 during excavation (10 days), linings installation (30 hours), and consolidation (10 days) steps.**

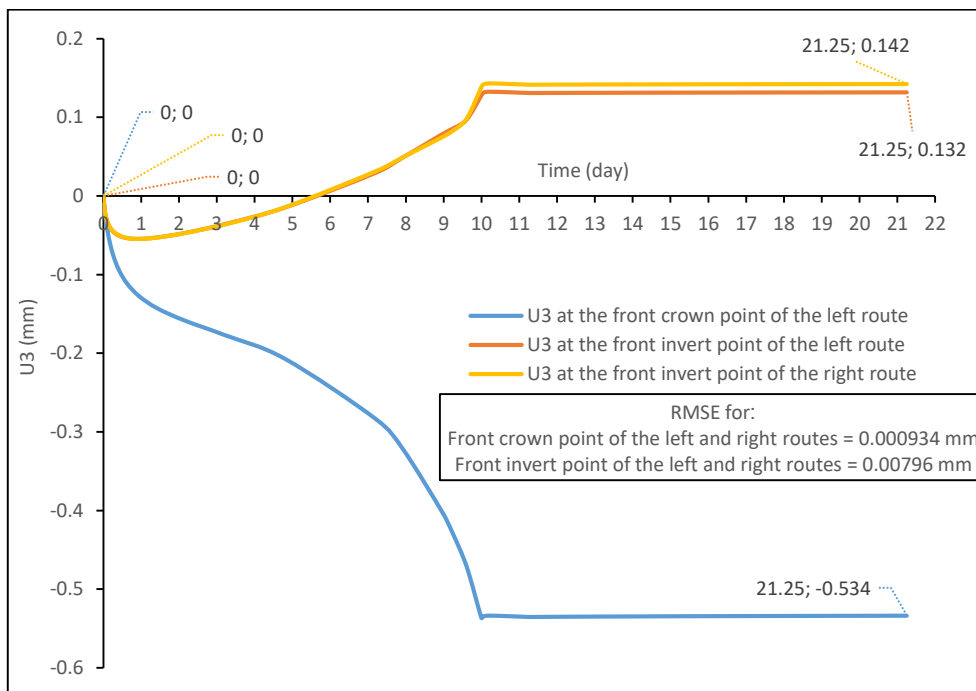


**Figure D.23: Change curves of the vertical displacements (U3) for the front faces of the left and right routes at location-6/line-2 during excavation (10 days), linings installation (30 hours), and consolidation (10 days) steps.**

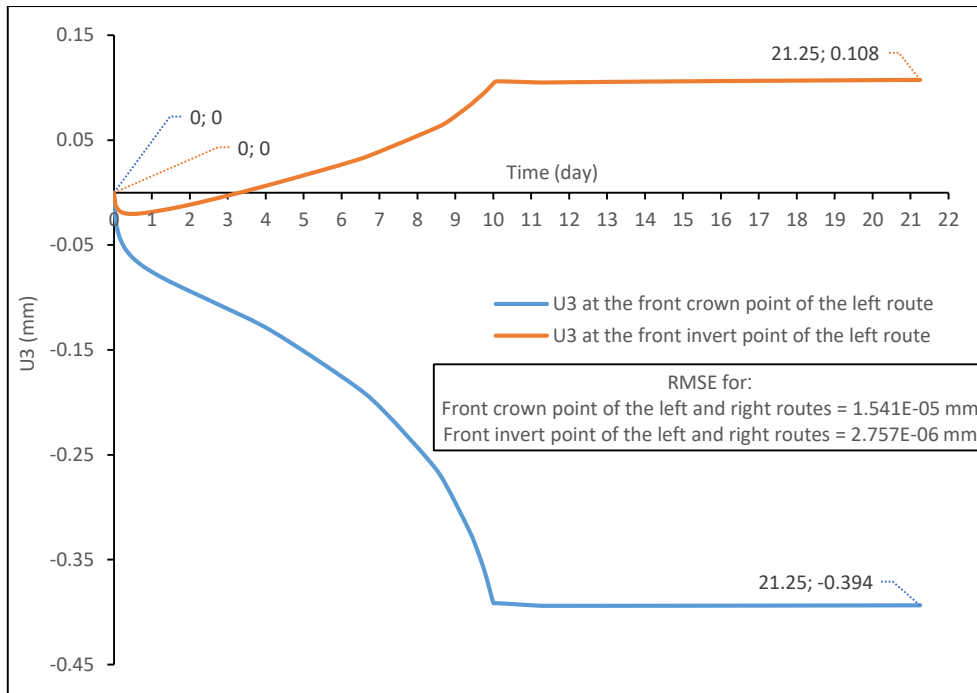


**Figure D.24: Change curves of the vertical displacements (U3) for the front faces of the left and right routes at location-7/line-2 during excavation (10 days), linings installation (30 hours), and consolidation (10 days) steps.**

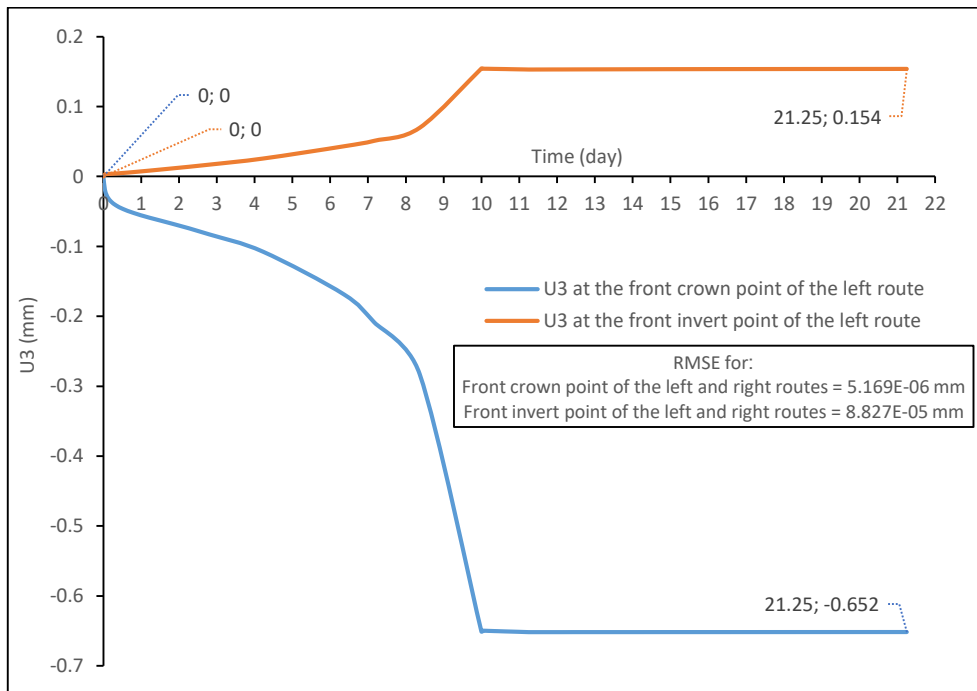
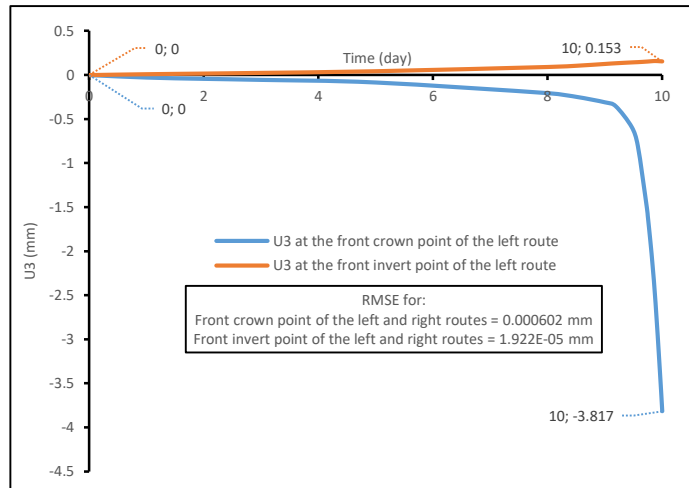
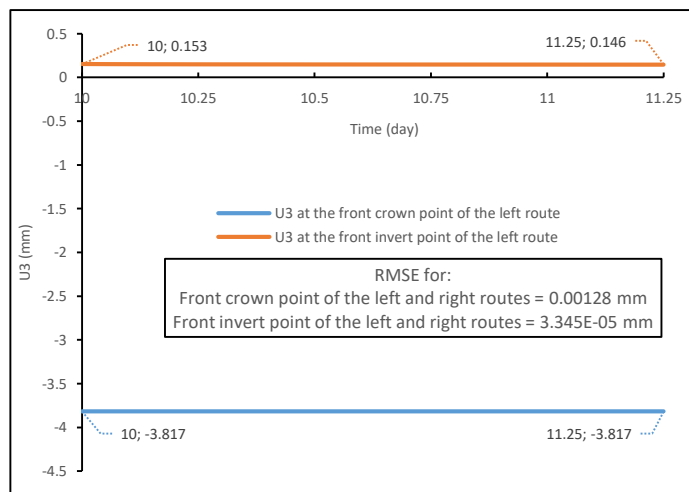


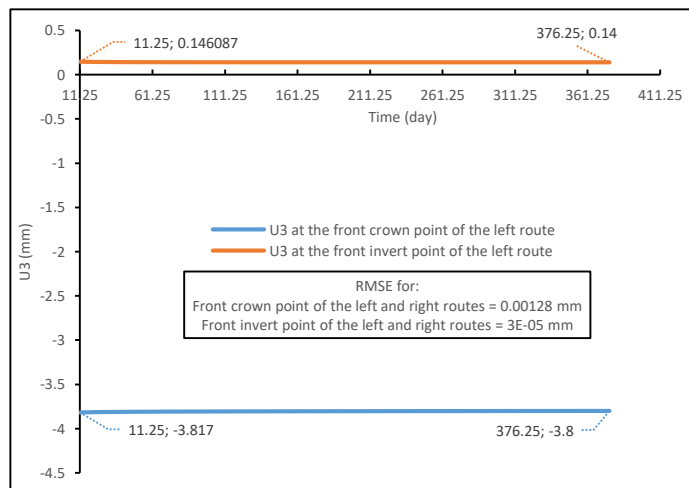
**Figure D.25: Change curves of the vertical displacements (U3) for the front faces of the left and right routes at location-8/line-2 during excavation (10 days), linings installation (30 hours), and consolidation (10 days) steps.**



**(A) Excavation step (10 days)**



**(B) Linings installation step (30 hours; 1.25 days)**



**(C) Consolidation step (1 year)**

**Figure D.26: Change curves of the vertical displacements (U3) for the front faces of the left and right routes at location-9/line-2 during excavation (10 days), linings installation (30 hours), and consolidation (1 year) steps.**

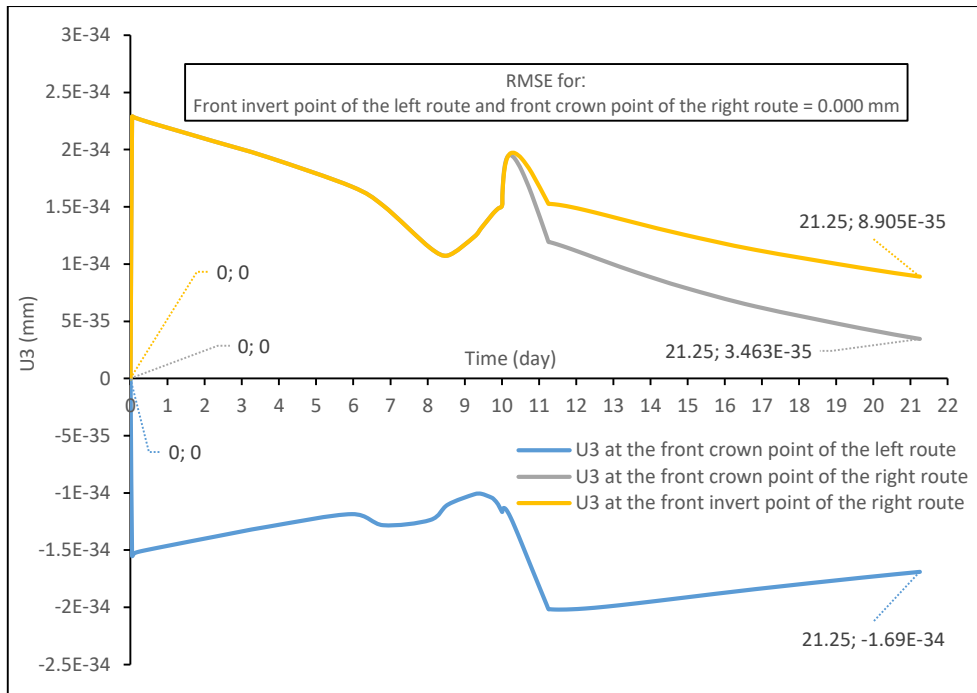
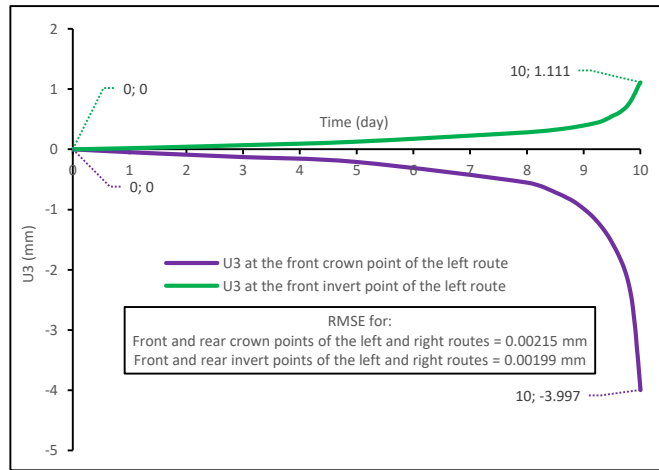
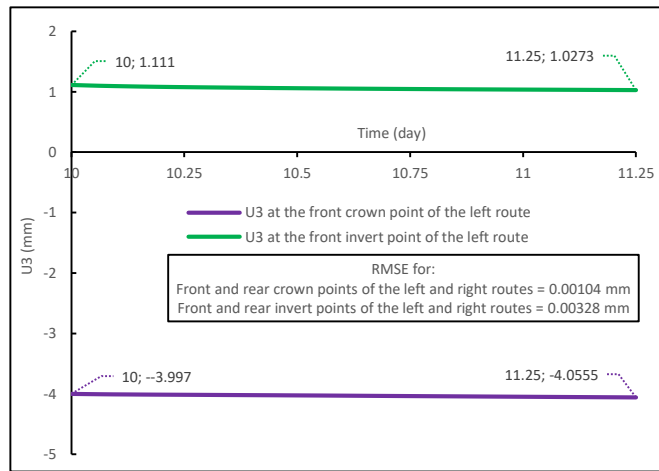


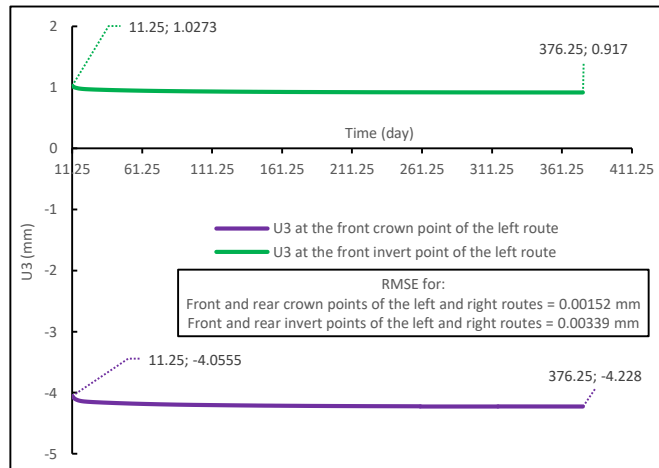
**Figure D.27: Change curves of the vertical displacements (U3) for the front faces of the left and right routes at location-10/line-2 during excavation (10 days), linings installation (30 hours), and consolidation (10 days) steps.**



**(A) Excavation step (10 days)**



**(B) Linings installation step (30 hours; 1.25 days)**



**(C) Consolidation step (1 year)**

**Figure D.28: Change curves of the vertical displacements (U3) for the front and rear faces of the left and right routes at location-11 (under Tigris)/line-2 during excavation (10 days), linings installation (30 hours), and consolidation (1 year) steps.**

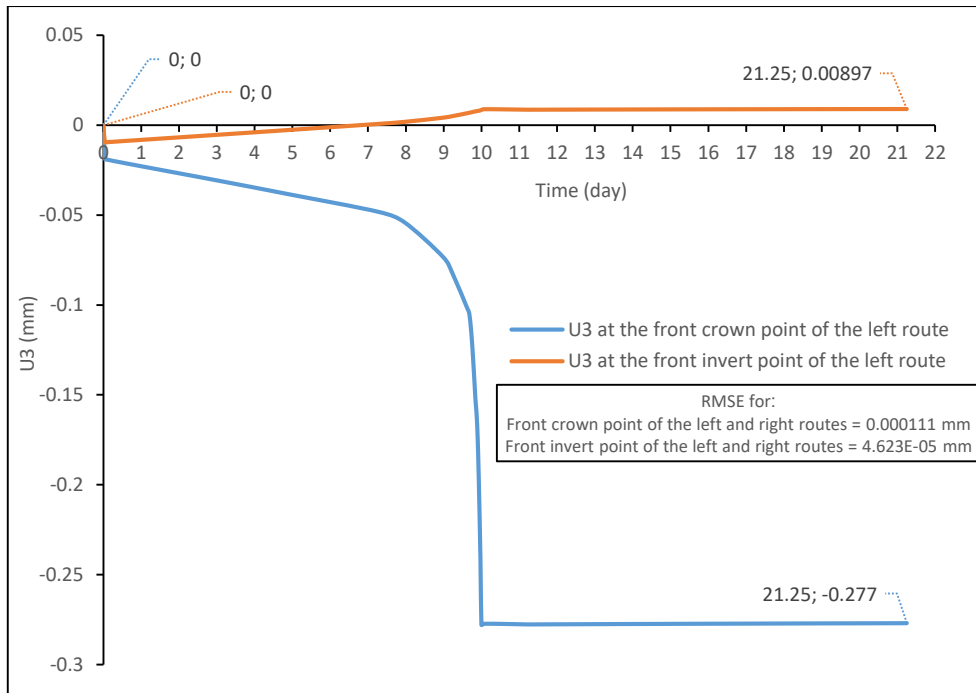


**Figure D.29: Change curves of the vertical displacements (U3) for the front faces of the left and right routes at location-12/line-2 during excavation (10 days), linings installation (30 hours), and consolidation (10 days) steps.**

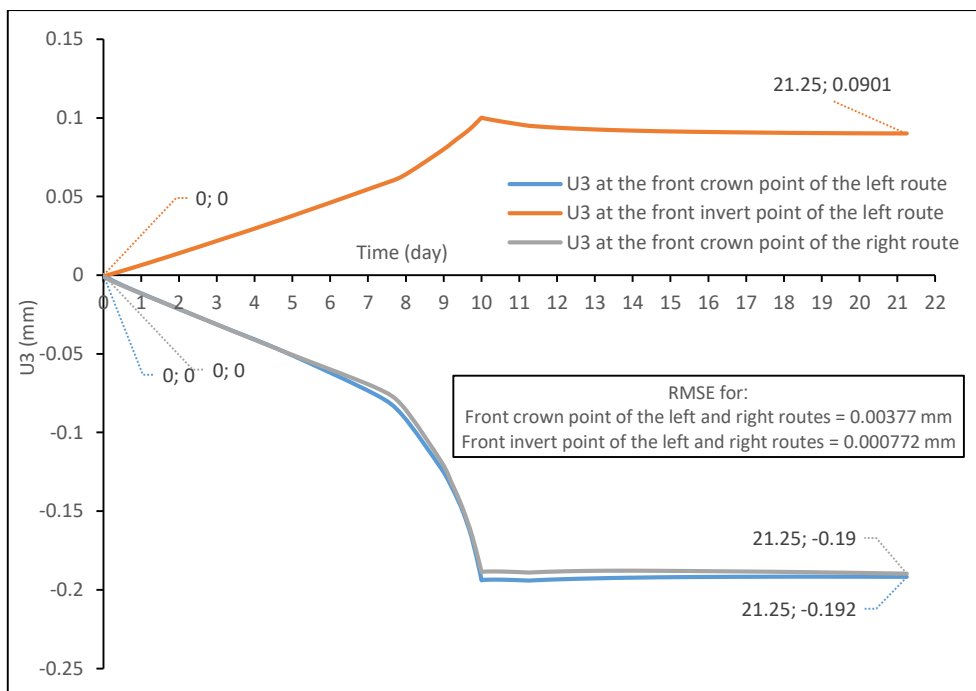


**Figure D.30: Change curves of the vertical displacements (U3) for the front faces of the left and right routes at location-13/line-2 during excavation (10 days), linings installation (30 hours), and consolidation (10 days) steps.**



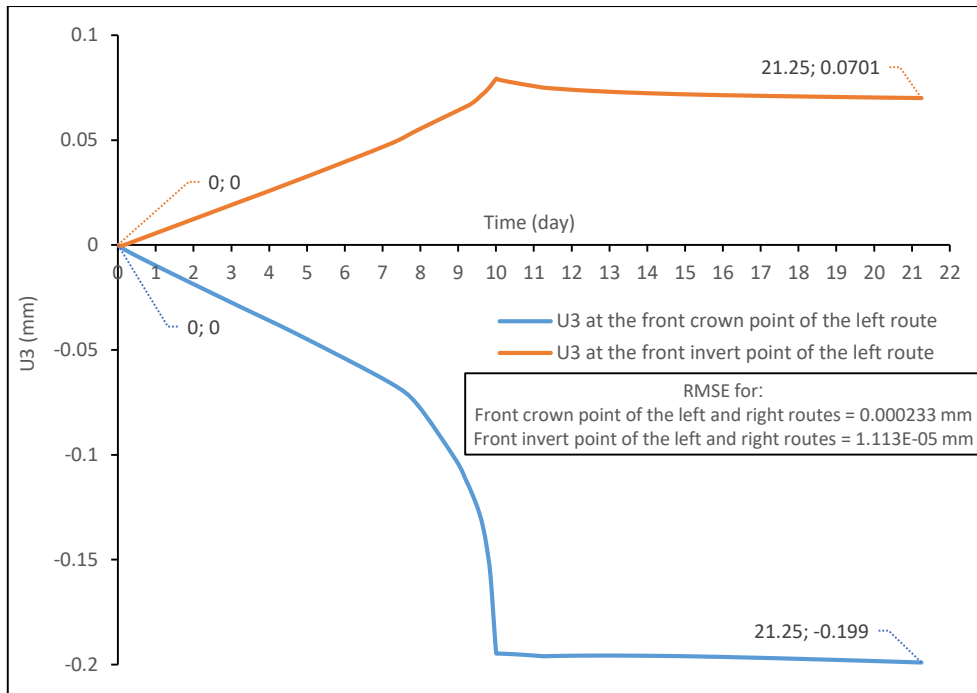


**Figure D.31: Change curves of the vertical displacements (U3) for the front faces of the left and right routes at location-14/line-2 during excavation (10 days), linings installation (30 hours), and consolidation (10 days) steps.**

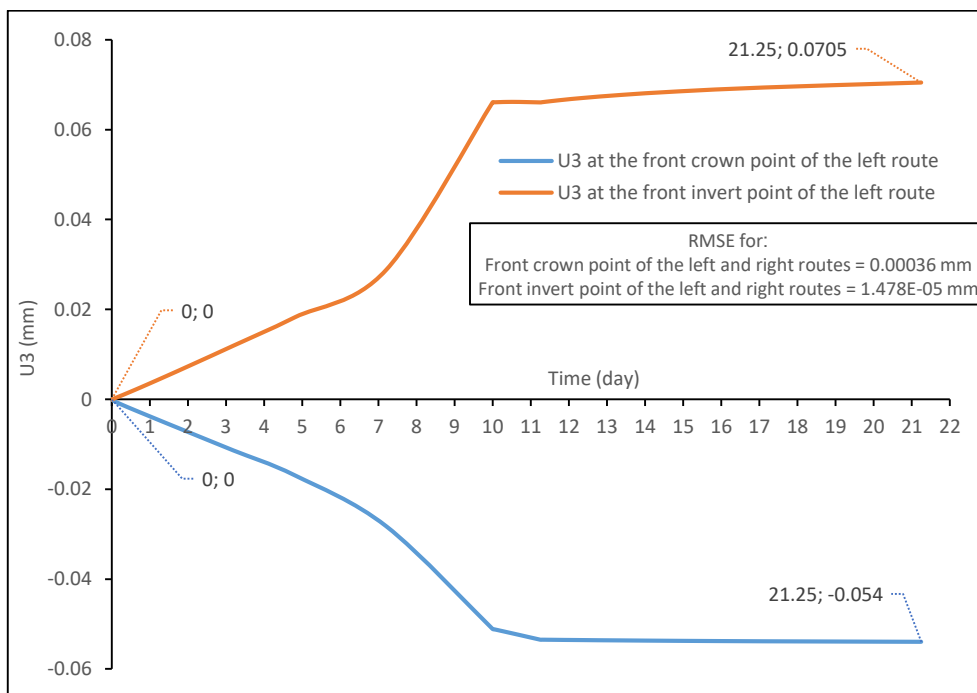


**Figure D.32: Change curves of the vertical displacements (U3) for the front faces of the left and right routes at location-15/line-2 during excavation (10 days), linings installation (30 hours), and consolidation (10 days) steps.**

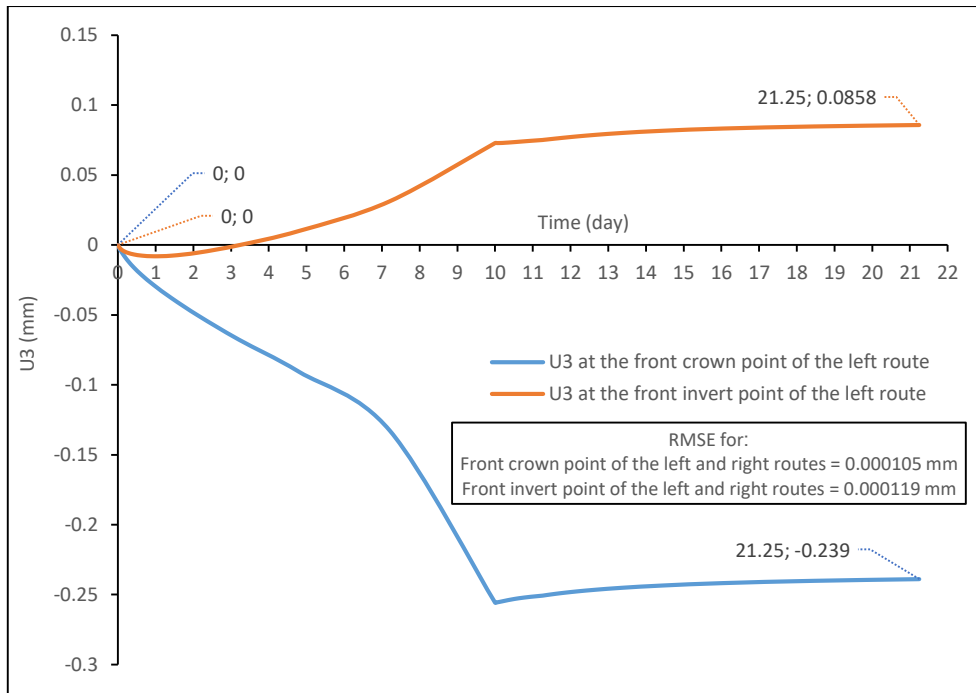


**Figure D.33: Change curves of the vertical displacements (U3) for the front faces of the left and right routes at location-16/line-2 during excavation (10 days), linings installation (30 hours), and consolidation (10 days) steps.**

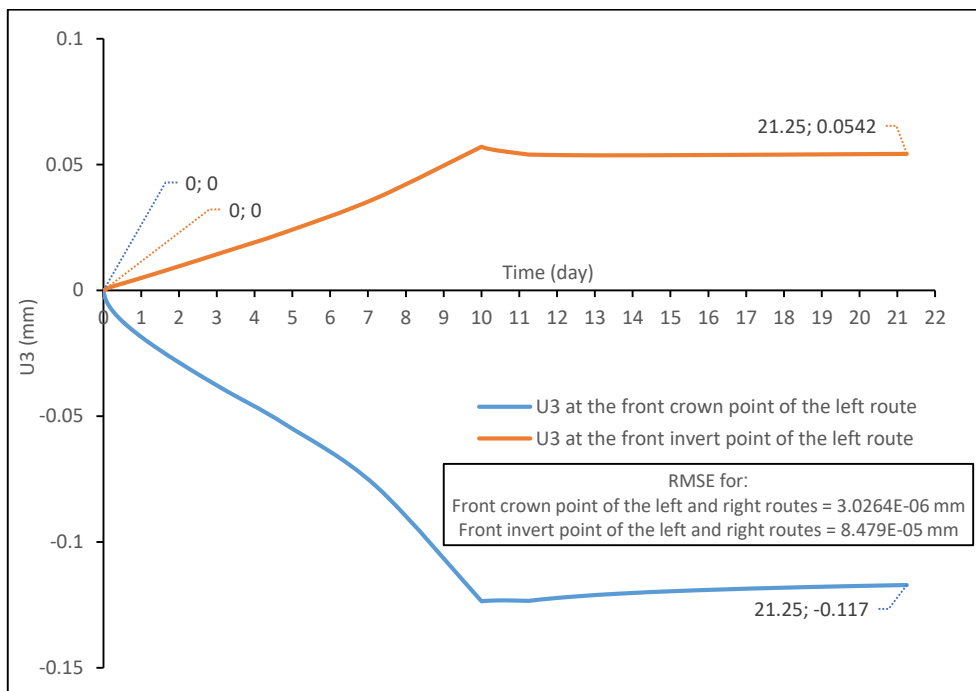


**Figure D.34: Change curves of the vertical displacements (U3) for the front faces of the left and right routes at location-17/line-2 during excavation (10 days), linings installation (30 hours), and consolidation (10 days) steps.**

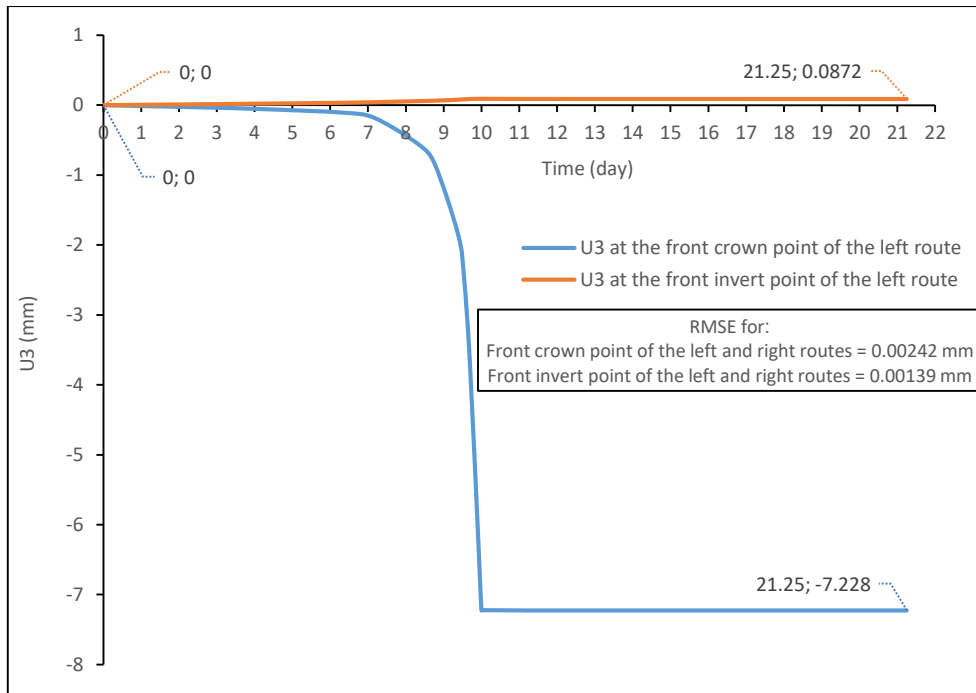


**Figure D.35: Change curves of the vertical displacements (U3) for the front faces of the left and right routes at location-18/line-2 during excavation (10 days), linings installation (30 hours), and consolidation (10 days) steps.**

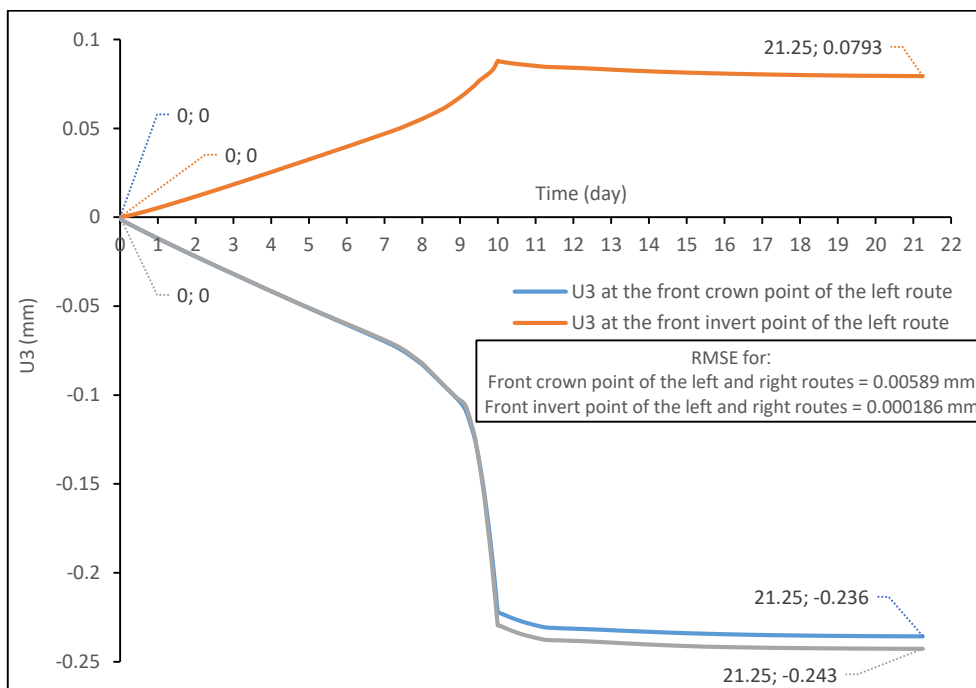


**Figure D.36: Change curves of the vertical displacements (U3) for the front faces of the left and right routes at location-19/line-2 during excavation (10 days), linings installation (30 hours), and consolidation (10 days) steps.**

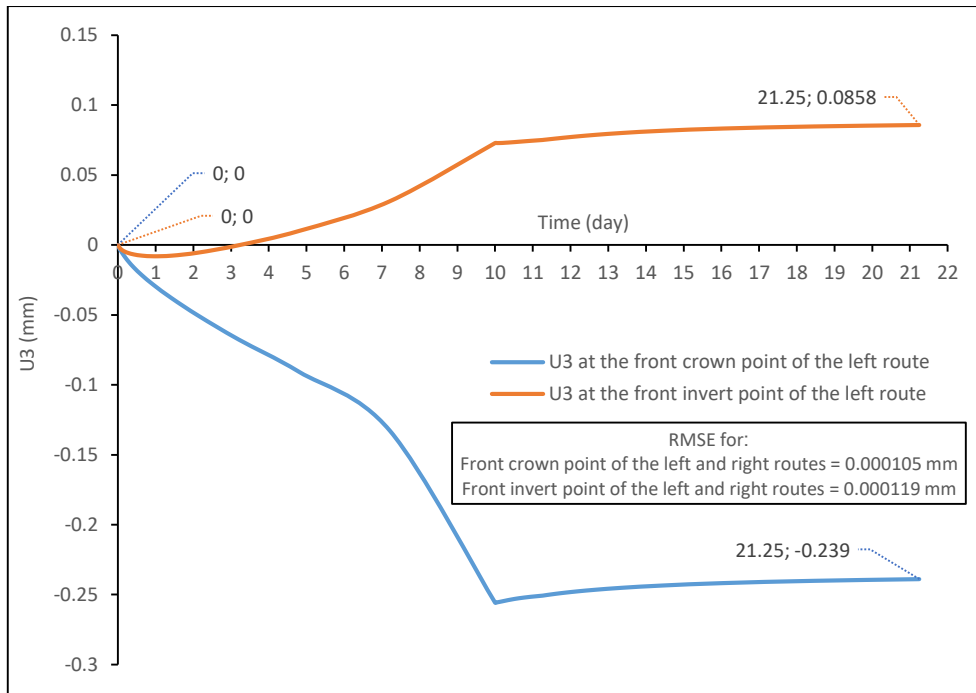


**Figure D.37: Change curves of the vertical displacements ( $U_3$ ) for the front faces of the left and right routes at location-20/line-2 during excavation (10 days), linings installation (30 hours), and consolidation (10 days) steps.**

٢ كنت ا م٢ من تلك الضغوط قبل عملية الحفر الناتجة من ارتفاع عمود ماء اعْتَبِرَ انه يساوي ٦ م ، ووجدَ ان عمق الماء في النهر قد رجع الى مستواه ما قبل عملية الحفر بعد سنة تقريبا من انتهاء عملية التثبيت ومستمر الى مدى بعيد من الزمن.

وجدَ في هذه الدراسة ان النموذج ثلاثي الابعاد الذي يربط كليا بين ضغط ماء المسام والاجهاد يمثل تمثيلا حقيقيا العلاقة بين نفق قطار بغداد المقترح والماء الجوفي، ولم تكن هناك مخاطر حدثت على سطح الارض وعمق ماء نهر دجلة عند كل النقاط المختاره.

## المستخلص

تم في هذه الدراسة إجراء تحليل عددي ثلاثي الأبعاد باستخدام طريقة العنصر المحدد للتنبؤ بالمتغيرات الحقلية للتربة المحيطة بنفق قطار بغداد المقترح الذي يتكون من خطين واقعين في مدينة بغداد ولكل خط يوجد مسارين للنفق. الخط الاول يقع في الرصافة والخط الثاني يمتد من الرصافة الى الكرخ. إستُخدِم "الاباكوس ٢٠١٦" لمحاكاة سلوك مساري النفق باستخدام نموذج ثلاثي الابعاد الذي يربط كليا بين ضغط ماء المسام والاجهاد عند ٣٨ موقع حيث تم اختيار ١٨ موقعا على الخط الاول و ٢٠ موقعا على الخط الثاني. تم تحديد اعماق المياه الجوفية عند هذه المواقع باستخدام افضل سطوح شبكية مكانية متولدة من ارتفاعات سطح الارض ومناسب المياه الجوفية الساكنة المسجلة عند ٢٠٦ بئر في محافظة بغداد وقد إستُخدِمَت حزمة برنامج نُظَم المعلومات الجغرافية "الأرك جي آي أس ١٠,٥" لهذا الغرض. وقد فُرضَ ان طبقات التربة تتصرف كمواد مرنة-لدنة ينطبق عليها معيار فنشل موهر-كولمب سوياً مع قاعدة الجريان غير المترافق وان البطانات الكونكريتية تتصرف تصرف مرن خطي.

في كل نموذج تمت محاكاة العمليات الفعلية لانشاء نفق قطار بغداد المقترح بصورة دقيقة لمراحل ماقبل، اثناء، وبعد الحفر باستخدام "طريقة تغيير النموذج" حيث إفتُرضَ بان النفق يُحفر بالكامل. تم حساب الازاحات العمودية للتربة المحيطة ببطانات مساري النفق في الاشكال المشوهة للنماذج الثلاثية الابعاد لتلك ال ٣٨ موقعا اثناء عملية حفر النفق وبعدها ووجدَ ان اكبر ازاحة عمودية باتجاه الاسفل حصلت عند نقاط التاج لمساري النفق عند الموقع-٨ على الخط الاول بالقرب من قناة الجيش بقيمة تساوي تقريبا ٤,٤ ١١ ملم في نهاية مرحلة الحفر واستمرت لفترة طويلة بعد انتهاء عملية التثبيت، وان اكبر ازاحة عمودية باتجاه الاعلى حصلت عند النقاط السفلية لمساري النفق في نفس الموقع بقيمة تساوي تقريبا ٦,٦ ١١ ملم في نهاية مرحلة الحفر واستمرت لفترة طويلة بعد انتهاء عملية التثبيت.

بخصوص نفق قطار بغداد المقترح المار تحت نهر دجلة، تم استخدام نموذج الموقع-١١ على الخط الثاني تحت نهر دجلة لحساب ضغوط ماء المسام عند التربة المحيطة ببطانات مساري النفقين وعند قعر النهر اثناء عملية حفر النفق وبعدها حيث تم أولاً: حساب ضغوط ماء المسام عند التربة المحيطة بالبطانتين في الشكل المشوه لهذا النموذج وتم ايجاد ان كل ضغوط ماء المسام عند انتهاء مرحلة الحفر هي ضغوط سالبة وضمن مدى يتراوح تقريبا من ٤,٤ كنت|م<sup>٢</sup> الى ٧,٧ كنت|م<sup>٢</sup> وفي نهاية مرحلة التثبيت كانت موجبة وضمن مدى يتراوح تقريبا من ١,٧٤٤ كنت|م<sup>٢</sup> الى ١٤٠ كنت|م<sup>٢</sup> و بعد سنة من انتهاء عملية التثبيت اصبحت تساوي تقريبا ٧,٧٣١٧ كنت|م<sup>٢</sup> على طول خطوط التاج لمساري النفقين و ٤٥,٣٨٣ كنت|م<sup>٢</sup> على طول الخطوط السفلية لمساري النفقين وتستمر الى الى مدى بعيد من الزمن. ثانياً: حساب ضغوط ماء المسام عند قعر النهر في الشكل المشوه لنفس النموذج للموقع -١١ على الخط الثاني تحت نهر دجلة اثناء عملية حفر النفق وبعدها وقد وجدَ ان كل ضغوط ماء المسام عند قعر النهر وعلى طول المسافة الواقعة بين مساري النفقين في نهاية مرحلة الحفر وانتهاء عملية التثبيت هي اصغر بمقدار



جمهورية العراق  
وزارة التعليم العالي والبحث العلمي  
الجامعة التكنولوجية  
قسم هندسة البناء والانشاءات



## تقييم تأثيرات ضغط المياه الجوفية حول نفق قطار بغداد

أطروحة  
مقدمة الى قسم هندسة البناء والانشاءات في الجامعة التكنولوجية  
كجزء من متطلبات نيل درجة دكتوراه فلسفة  
في هندسة الموارد المائية

من قبل

**معمر حازم علي الطائي**

(ماجستير هندسة موارد مائية)

باشراف

**أ. د. عقيل شاكر العادلي**

**أ. م. د. ناكرتنام سيفاكوكان | جامعة جيمس كوك | استراليا**

كانون الثاني ٢٠١٨ م

ربيع الثاني ١٤٣٩ هـ